Assessing the mixing effectiveness of dual-impeller systems in the agitation of viscoplastic fluids

Andrew W Russell, Lyes Kahouadji, Seungwon Shin, Jalel Chergui, Damir Juric, Patrick M. Piccione, Omar K. Matar, Paul F Luckham, Christos N. Markides

Assessing the mixing effectiveness of dual-impeller systems in the agitation of viscoplastic fluids

Andrew W. Russell[1], Lyes Kahouadji[1], Seungwon Shin[2], Jalel Chergui[3], Damir Juric[3], Patrick M. Piccione[4,5], Omar K. Matar[1], Paul F. Luckham[1], Christos N. Markides[1]

[1] Department of Chemical Engineering, Imperial College London, London SW7 2AZ, U.K.

[2] Department of Mechanical and System Design Engineering, Hongik University, Seoul 04066, Republic of Korea.

[3] Laboratoire d'Informatique pour la Mécanique et les Sciences de l'Ingénieur (LIMSI), Centre National de la Recherche Scientifique (CNRS), Université Paris Saclay, Bât. 507, Rue du Belvédère, Campus Universitaire, 91405 Orsay, France.

[4] Process Studies Group, Technology & Engineering, Syngenta, Breitenloh 5, Münchwilen, CH-4333, Switzerland

[5] F. Hoffmann-La Roche AG, Grenzacherstrasse 124, 4070 Basel, Switerland

Email: c.markides@imperial.ac.uk

Abstract: Dye visualisation techniques and CFD are employed to examine the flow of viscoplastic Carbopol™ 980 fluids, agitated with dual-impeller systems comprising various combinations of Rushton turbine (RT) and pitched blade turbine (PBT) impellers. The effects of impeller configurations and arrangements on the flows are investigated. Phenomena including mixing, 'cavern'-'cavern' segregation, and flow compartmentalisation are explained by considering the dynamics of the velocity fields and associated flow patterns. Dual-RT agitation induces highly symmetrical flows and dependent on the impeller separation, produces strong, time-dependent flow compartmentalisation. Flow compartmentalisation is overcome in comparable dual-PBT systems due the downward-pumping nature of the PBT producing a state of full-tank homogeneity through a cavern engulfment process. The quality of mixing is compared with mixing effectiveness being maximised for a configuration featuring PBT overlying RT impellers. These results demonstrate clearly the influence of the impeller geometrical arrangement on the mixing effectiveness of viscoplastic fluids in dual-impeller systems.

Keywords: *Caverns, dual-impeller, homogeneity, mixing effectiveness, stirred vessels, viscoplastic*

1. Introduction

Mixing-based unit operations are often utilised in the chemical sector. The materials used in relevant processes are often associated with complex rheological properties, along with high levels of reactivity, handling difficulty and cost. Carbopol fluids have been shown to be suitable replacement model fluids for scaled-down processes, as they are safe, easy-to-handle, inexpensive, but most importantly have the desired viscoplastic rheological properties (Russell *et al.* (2019)). Viscoplastic fluids exhibit a yield stress, which once exceeded flow with shear-thinning characteristics, and are commonly described by the mathematical Herschel-Bulkley model (Eq. 1) (Herschel and Bulkley (1926); Papanastasiou (1987); Balmforth *et al.* (2014); Dinkgreve *et al.* (2016); Malkin *et al.* (2017)):

$$\tau = \tau_{\mathrm{y}} + K\dot{\gamma}^{n} \tag{1}$$

where τ, τ_{y}, K, $\dot{\gamma}$, and n are the shear stress, yield stress, flow consistency index, shear rate, and flow behaviour index, respectively.

When these materials are mixed in vessel systems equipped with a central impeller, a '*cavern*' can form; this corresponds to a region of flow surrounding the central impeller in which the impeller-induced stress exceeds the material yield stress. Outside of this region, the material is stagnant and exhibits solid-like behaviour (Solomon *et al.* (1981); Wichterle and Wein (1981); Elson *et al.* (1986); Arratia *et al.* (2006)). Various authors have investigated how operating conditions, such as impeller rotational speed, N, fluid rheology, impeller geometry and vessel design impact the flow dynamics of viscoplastic fluids in stirred vessels, via both numerical simulations and experiments (Solomon *et al.* (1981); Elson *et al.* (1986); Elson (1988); Galindo and Nienow (1992, 1993); Hirata *et al.* (1994) Jaworski *et al.* (1994); Galindo *et al*. (1996); Amanullah *et al.* (1997, 1998a, 1998b); Arratia *et al.* (2006); Adams and

Barigou, (2007); Ihejirika and Ein-Mozaffari (2007); Pakzad *et al.* (2008a, 2008b, 2008c, 2013b, 2013c); Saeed *et al.* (2007, 2008); Saeed and Ein-Mozaffari (2008); Hui *et al.* (2009); Patel *et al.* (2012); Sossa-Echeverria and Taghipour (2014, 2015); Kazemzadeh *et al.* (2016); Cortada-Garcia *et al.* (2018)).

The mixing of viscoplastic fluids in vessels equipped with multi-impeller systems, including coaxial mixers, in an attempt to maximise mixing performance, has been investigated by numerous authors. Coaxial impellers incorporate both small, central impellers (e.g. Rushton turbines (RT), Scaba impellers, pitched-blade turbines (PBT) and propellers) and close-clearance impellers (e.g. anchors, helical ribbons and Maxblend impellers), with both impeller types being fitted on either the same or separate shafts. In a series of studies, Pakzad *et al.* (2013a, 2013b, 2013c) looked at the agitation of Xanthan gum (XG) solutions with various coaxial systems, using electrical resistance tomographic (ERT) techniques in conjunction with computational fluid dynamics (CFD) simulations. In the first two studies, Pakzad *et al.* (2013a, 2013b) used a Scaba-anchor impeller system for agitation, and the effects of fluid rheology and speed ratios between the two impellers on mixing time, flow patterns and power consumptions were considered. Pakzad *et al.* (2013c) then compared the mixing efficiency of an ASI impeller (a combination of a PBT and a Scaba impeller) to that of an RT impeller, an axial-radial impeller (ARI) and an axial PBT impeller. The ASI impeller was the most efficient mixer, with mixing efficiency being enhanced when combined with an anchor in a coaxial system. In a subsequent study, Kazemzadeh *et al.* (2016a) used ERT and CFD to study the impact of fluid rheology and defined impeller ratios on the mixing performance (in terms of mixing time and power consumption) of a Scaba-anchor coaxial mixer on the agitation of XG solutions. In two further studies, Kazemzadeh *et al.* (2016b, 2017) looked at the mixing performance (in terms of mixing time and efficiency) of coaxial mixers comprising of a wall-scraping anchor and different dual, central impellers (RT, Scaba and PBT impellers) when agitating XG solutions.

In an industrial setting, it is desirable to aim to achieve 'complete' mixing, where the entirety of the vessel contents is in motion and no stagnant zones exist, to minimise losses and product degradation, whilst maximising economic gains and product yield. Coaxial mixers are often used on smaller scales to invoke this state, however, at larger scales, combinations of central impellers are utilised, due to the unfeasibly high power consumptions and costs associated with close-clearance impellers. Several authors have assessed the mixing performance of multiple small, central impeller systems in the agitation of materials ranging from simple Newtonian (Baudou *et al.* (1997); Jaworski *et al.* (2000); Vrabel *et al.* (2000); Bujalski *et al.* (2002); Montante and Magelli (2004); Aubin and Xuereb (2006)) to complex non-Newtonian (shear-thinning and viscoplastic) fluids.

Kelly and Humphrey (1998) used CFD simulations to study the impact of N, fluid rheology and the distance between a cooling coil bank and fermentor wall, on the flow of viscous shear-thinning fluids in a 75 m^3 fermenter equipped with three axial Lighnin A315 impellers (impeller diameter-to-tank diameter ratio, $D/T = 0.45$). Greater N were required to minimise stagnant zones when n increased from 0.2 to 0.6, at constant K = 25 Pa s^n. Alvarez *et al.* (2002) used planar laser-induced fluoresence (PLIF), UV visualisation and numerical simulations to study the mechanisms of development and evolution of mixing structures and flow patterns in laminar Newtonian and non-Newtonian flows, agitated by single and 3-stage discs, standard 6-blade RTs and modified 3-blade RTs (all $D/T = 0.32$). The presence of blades in the RT impellers produced choatic flow in the Newtonian fluids, compared to the 2-D flows resulting from disc agitation. In the non-Newtonian flows, spontaneous chaos occurred when mixing with all impeller types and configurations. Letellier *et al.* (2002) used CFD to analyse flows in Newtonian and shear-thinning fluids over three geometrically-similar scales (0.03, 3.8 and 11.5 m^3). Agitation occurred with an industrial dual-impeller system: a MIG double-flux impeller ($D/T = 0.9$) situated above a 4-blade PBT impeller ($D/T = 0.6$). There were large variations in the flow dynamics and patterns when scaling at constant energy per volume, and breaking geometrical similarity or modifications to the stirring system was suggested as a method to reduce the variations in flow patterns over scales.

There have been some studies investigating the mixing of viscoplastic fluids in vessels equipped with multiple, central impellers. In an early study, Solomon *et al.* (1981) used hot-film anemometry (HFA) and flow visualisation techniques to investigate the flow patterns in XG, Carbopol and carboxymethyl cellulose (CMC) solutions, agitated with RT impellers ($D/T = 0.33$ and 0.50) alone and in conjunction with 6-bladed PBT impellers ($D/T = 0.33$ and 0.50). The specific power input required to achieve

complete mixing was dramatically reduced using the dual-PBT-RT impellers, compared to the single RT systems. For both the single- and dual-impeller systems, the larger impellers required lower power inputs to achieve well-mixed systems. Galindo *et al.* (1996) evaluated the mixing performance of single- and dual-RT and 1- and 2-stage Intermig (all D/T = 0.53) impellers using dye visualisation methods. The single RT produced larger caverns than the 1-stage Intermig impeller at low power drawn in a Carbopol 940 (C940) solution, but comparable caverns at higher power drawn, with a limit in cavern volume of ~40% the total liquid volume. Similar trends were observed in the respective dual systems, with ~90% cavern volume being attained at higher power drawn values. Amanullah *et al.* (1998) assessed the mixing performance of four pairs of impellers: standard 6-blade RT (D/T = 0.33), large 6-blade RT (D/T = 0.42), SCABA 6SRGT impellers (D/T = 0.54) (all radial flow) and axial Prochem Maxflo T impellers (D/T = 0.44), in a 150 L fermenter containing a XG fermentation. The standard RT was inferior to the other three impeller types, with large diameter, low power number impellers (Prochem Maxflo T and SCABA 6SRGT) being favoured for enhanced XG productivity and reduced costs. Arratia *et al.* (2006) investigated the mixing of Newtonian (glycerin) and viscoplastic (0.1 wt% C940) fluids using tracer visualisation techniques (PLIF and UV fluorescence), particle image velocimetry (PIV) to obtain 2-D velocity fields and CFD. Agitation occurred using single RT or 3-RT configurations (all D/T = 0.31, impeller separation and clearance = 0.38T) and detailed mixing structures and flow characteristics were obtained. Both experiment and CFD captured the key flow features, including cavern formation and distinct cavern-cavern segregation in the 3-RT systems. Breaking spatial symmetry weakened the segregation and resulted in better mixing between caverns. Xiao *et al.* (2014) used CFD to evaluate the mixing of low yield stress viscoplastic fluids by single and dual 6-blade PBT systems (D/T = 0.33) and developed a model to predict cavern shape and size in these systems. The caverns adopted a toroidal shape when agitated by a single PBT, which developed from a 'horn' torus to an 'apple' torus as Reynolds number, *Re* increased. In the dual-PBT system, CFD simulations at different impeller spacings, G (G = 0.60-1.40D) were conducted at constant *Re*. With increased G, more fluid in the upper region of the vessel was agitated by the upper PBT, leading to increased total cavern volumes. At high *Re*, the caverns again adopted an apple torus morphology. Ameur *et al.* (2015) numerically studied the effect of multiple operating conditions on the mixing of various XG solutions by 1-, 2- and 3-Scaba 6SRGT (D/T = 0.50) impeller systems and showed that mixing performance was maximised (stagnant zones minimised) using the 3-impeller system.

Reviewing the existing literature has shown that using multi-impeller systems for mixing a range of fluids (from Newtonian to viscoplastic) has been well studied. However, limited studies have looked at using a combination of different impeller types for the agitation of viscoplastic fluids, with the aim of optimising the system to enhance mixing effectiveness and achieve homogeneity throughout the vessel. In a recent study, Russell *et al.* (2019) used dye visualisation and CFD to assess the mixing in Carbopol 980 (C980) fluids over three scales with geometrically-similar RT impellers. For the scales and fluids investigated, a scaling method for matching dimensionless cavern sizes was proposed, and comparisons were made between the flows produced by agitation with RT and PBT impellers of similar dimensions. In the current study, the same experimental and numerical techniques will be used to evaluate the mixing performance of dual-impeller systems in the agitation of C980 fluids. The mixing system will comprise a 2 L vessel and a combination of RT and PBT impellers, with the impeller configuration that is able to most effectively minimise stagnant zones, flow segregations and produce full-tank homogeneity, being determined.

In what follows, Sections 2 and 3 outline the experimental and numerical methods used in this work, respectively. This is followed by a presentation of the results in Section 4, along with an accompanying discussion, followed by a summary of the main conclusions in Section 5.

2. Experimental methods

2.1 Formulation and rheological characterisation of C980 fluids

Carbopol 980 (C980, Lubrizol Corporation) fluids were used as the test viscoplastic fluids throughout this study. Carbopol is based on the polyacrylic acid structure and has the capacity to swell in aqueous media to form a non-thixotropic microgel. Swelling is enhanced in basic media through the ionisation of carboxylic

acid groups to carboxylate groups, leading to strong mutual repulsions between the polymer chains within the microgel particles. The result is fluids with strengthened viscoplastic properties and improved optical clarity (Barry and Meyer (1979); Oppong *et al.* (2006); Piau (2007); Russell *et al.* (2019)).

In this study, three C980 fluids were formulated. C980 powder (0.15 wt%) was dissolved in deionised water via mechanical agitation, and on complete dissolution, small quantities of 2 wt% NaOH(aq) solution were added, so that each fluid was at pH 6.40-7.40. The fluids were rheologically characterised using a shear stress-controlled Anton Paar MCR 302 rheometer, equipped with a roughened cone-and-plate geometry (12.6 μm roughness, 0.998° cone angle, cone and plate diameter = 50 mm, CP50-1-41592). All fluids underwent shear stress down-sweep measurements (60 pt dec^{-1}, 5 s pt^{-1}) and the resulting flow curves were mathematically fitted to the Herschel-Bulkley model (Eq. 1). For each rheological measurement performed in this study, the range of shear rate values (~0.001-1000 s^{-1}) investigated ensured that the resulting full range of shear rates (and shear stresses) in the mixing vessel systems were accounted for. The viscoelastic properties of C980 fluids have been studied, and depending on pH, the storage modulus, *G'* typically ~400 Pa and the loss modulus, *G''* typically ~30 Pa. The rheological and physical properties of fluids used in this study can be seen in Table 1, along with a summary of which fluid corresponds to mixing study. From Table 1: *Mixing Study A* relates to mixing with a dual-Rushton turbine (dual-RT) system; *Mixing Study B* relates to mixing with a dual-pitched-blade turbine (dual-PBT) system; and *Mixing Study C* relates to mixing with a system comprising of one Rushton turbine and one pitched-blade turbine (RT-PBT).

Table 1. Physical and Herschel-Bulkley rheological properties (including the approximate errors associated with the parameters) of the fluids used in each of the mixing studies in this work.

		Fluid Composition and Physical Properties			**Herschel-Bulkley Rheological Properties**		
Mixing Study	**Impeller System**	**C980 Mass Fraction / wt%**	**Fluid pH**	**Fluid Temperature / °C**	**Yield Stress, τ_y (± ~7%) / Pa**	**Flow Consistency Index, *K* (± ~10%) / Pa s^n**	**Flow Behaviour Index, *n* (± ~5%)**
A	dual-RT	0.15	6.40	25.6	28.1	5.7	0.46
B	dual-PBT	0.15	6.62	24.6	27.7	6.2	0.46
C	RT-PBT	0.15	7.40	23.4	32.6	8.6	0.43

2.2 Stirred vessel system and experimental procedures

An unbaffled, cylindrical vessel system, with a quoted tank volume of 2 L and tank diameter, T = 0.148 m was used throughout this study. The two impeller types were 6-bladed RTs and 4-bladed 45° PBTs, each with diameters, D = 0.041 m and hence a D/T = 0.28. The impellers were fitted to a shaft, with shaft diameter-to-impeller diameter, S/D = 0.24 and the shaft-impeller system was centrally mounted onto an IKA EUROSTAR 60 motor. For each mixing study, the liquid fill height, H_L = 0.135 m (H_L/D = 3.29) and the clearance for lower of the two impellers, C_2 = 0.045 m (C_2/D = 1.10). The clearance for the upper of the two impellers, C_1 = 0.095 m (C_1/D = 2.32) or 0.075 m (C_1/D = 1.83), depending on the system in question, resulting in an impeller separation, G = 0.05 m (G/D = 1.22) or 0.03 m (G/D = 0.73), respectively. A schematic of the mixing system and details relating to each of the mixing studies can be found in Figure 1 and Table 2, respectively. Dimensions G, C_1 and C_2 were measured from the centre of each of the impellers, as highlighted in Figure 1.

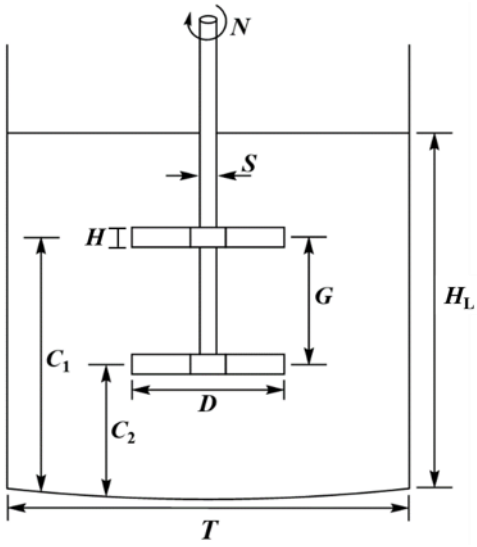

Property	Symbol
Impeller rotational speed, N	$N = 0.0–33.3$ s^{-1}
Tank volume, V	$V = 2$ L
Tank diameter, T	$T = 0.148$ m
Impeller diameter, D	$D = 0.041$ m
Impeller height, H	$H = 0.008$ m
Shaft diameter, S	$S = 0.24D$
Liquid fill height, H_L	$H_L = 3.30D$
Upper impeller clearance, C_1	See Table 2
Lower impeller clearance, C_2	$C_2 = 1.10D$
Impeller separation, G	See Table 2

Figure 1. Details and schematic of the experimental and numerical dual-impeller tank setup and geometry used throughout this work. Dimensions G, C_1 and C_2 are measured from the centre of each impeller.

Table 2. Details of the experimental setups used for each of the mixing studies reported in this work.

Mixing study	Upper impeller	Lower impeller	Upper and lower impeller diameter, D / m	Dimensionless upper impeller clearance, C_1/D	Dimensionless upper impeller clearance, C_2/D	Dimensionless impeller separation, G/D
A(1)	RT	RT	0.041	2.32	1.10	1.22
A(2)	RT	RT	0.041	1.83	1.10	0.73
B(1)	PBT	PBT	0.041	2.32	1.10	1.22
B(2)	PBT	PBT	0.041	1.83	1.10	0.73
C(1)	RT	PBT	0.041	2.32	1.10	1.22
C(2)	PBT	RT	0.041	2.32	1.10	1.22

For each mixing study, the fluid was loaded into the vessel, the impeller was set to a rotational speed, N = 4.2 s^{-1} and 2-3 mL of food dye (Sainsbury's Supermarkets Ltd) was injected at the tip of each impeller. For each mixing study where G = 0.05 m (G/D = 1.22, *Mixing Studies A(1), B(1), C(1) and C(2)*), blue food dye was injected at the tip of the lower impeller and green food dye was injected at the upper impeller tip. For the studies where G = 0.03 m (G/D = 0.73, *Mixing Studies A(2) and B(2)*), this was reversed. N was then incrementally increased up to 2000 rpm (33.3 s^{-1}), with images taken (Panasonic HDC-SD90/Apple iPhone 7 camera (12 megapixel resolution)) at each speed after 30 s, to capture the caverns at their equilibrium shape and size. In each mixing study, the cavern boundary was defined by the distinct transition from dyed to non-dyed material, which showed a clear demarcation on the images generated in our experiments. The dimensions of the RT and PBT impellers used in this work can be found in the Supplementary Information (Figure S.1 and Table S.1).

2.3 Error analysis

The main sources of error in this work are likely to be associated with the fluid formulation and rheological characterisation procedure, the mixing process itself possibly caused by the difficulties controlling the entrainment of air within the samples being characterised, and the errors associated with weighing out the various quantities of each material used to formulate the fluids. For a full error quantification, please see the work by Russell *et al.* (2019).

2.4 Dimensionless parameters

The key dimensionless parameters describing the flow of viscoplastic fluids in stirred vessel systems can be attained through dimensional analysis. The important parameters include the modified power-law Reynolds number, Re_m (Eq. 2), the yield stress Reynolds number, Re_y (Eq. 3), a dimensionless shear rate, $\bar{\dot{\gamma}}/N$, and flow behaviour index, n. Here, Re_m is the ratio of inertial to viscous forces and provides an indication of the flow regime in the cavern, whilst Re_y is a dimensionless fluid yield stress term, which will have a bearing on cavern size.

$$Re_m = \frac{\rho N^{2-n} D^2}{K} \tag{2}$$

$$Re_y = \frac{\rho N^2 D^2}{\tau_y} \tag{3}$$

$$\bar{\dot{\gamma}} = k_s N \tag{4}$$

When in the laminar flow regime (which was the case for all mixing studies in this work), the Metzner-Otto correlation (Eq. 4) can be utilised: $\bar{\dot{\gamma}}/N = k_s$ (Metzner and Otto (1957)). k_s has a weak dependence on impeller type and size, and values of 11.5 and 13, for RT and PBT impellers respectively, are deemed as appropriate (Metzner *et al.* (1961)). From Eq. 2-4, ρ, g and k_s are fluid density, gravitational acceleration and the impeller geometry constant, respectively, with all other variables having been previously defined. Russell *et al.* (2019) demonstrated that when mixing specific C980 fluids over different scales with a single impeller, key geometrical ratios, including *C*/*D*, *S*/*D* and *H*/*D*, should remain constant, and for given systems where the impeller is far enough from the interface for it to remain unperturbed, a relationship was developed, using the dimensionless parameters listed above, for scaling these systems to achieve flow similarity. This relationship will not be used in this study as it is only applicable to single-impeller systems.

3. Numerical methods

3.1 Numerical construction of the mixing system

The mixing system configuration considered in this study consists of a fixed cylindrical tank and a rotating impeller (a 6-bladed RT and/or a 4-bladed 45° PBT). The construction of both impeller and tank was performed using a similar approach to that followed by Kahouadji *et al.* (2018) that circumvents the need for time-consuming construction, meshing and re-meshing of any geometrical shape. Instead, the authors proceed in a modular manner, with the geometry being built from primitive geometrical objects using a state distance function that takes into account the interaction between these objects and the flow for both single (as in the current study) and two-phase flows (Kahouadji *et al.* (2018)). The final structure in the computational domain, visualised in Figure 2, consists of the iso-value $(x, y, z) = 0$; the static distance function, $\Psi(x, y, z)$ is positive for the fluid part and negative for the solid part, where (x, y, z) are Cartesian coordinates. Many primitive solid geometries are incorporated into the code, including spheres, planes, cylinders and tori, as are geometrical operations, such as "union" and "intersection" for each primitive object. In this study, only planes, cylinders and a combination of the two are required for the construction of the mixing system. As a first step, the geometrical shape for the system is chosen. For the case of the tank, a vertical cylinder with a radius, $R = 0.074$ m, was selected, where its distance function $\Psi_{cyl}(x, y, z) > 0$ for all Cartesian points that satisfy $(x - x_0)^2 + (y - y_0)^2 < R^2$, with (x_0, y_0) denoting the central axes within the tank. The bottom of the tank is closed off through calling another distance function, $\Psi_{pl}(x, y, z) > 0$ for all Cartesian points that satisfy $z > 0$. The resulting distance function characterising the cylindrical tank is performed by applying the intersection operation $\Psi_{tank} = \Psi_{cyl} \cap \Psi_{pl}$. Finally, the resulting construction of the open-top cylindrical tank is made when the isovalue, $\Psi_{tank} = 0$, as seen in Figure 2(a). Similarly, all parts of the impellers

(Ψ_{shaft}, Ψ_{hub}, Ψ_{disc} and Ψ_{blades}) were constructed and the union operator was used to produce the resulting distance function characterising each impeller. For the RT impeller: $\Psi_{RT} = \Psi_{shaft} \cup \Psi_{hub} \cup \Psi_{disc} \cup \Psi_{blades}$ and for the PBT impeller: $\Psi_{PBT} = \Psi_{shaft} \cup \Psi_{hub} \cup \Psi_{blades}$. Due to the lack of a disc, the Ψ_{disc} function can be neglected for the PBT. The numerical construction of these two impeller types can be seen in Figure 2(b), whilst Figure 2(c) shows the entire mixing system for a dual-PBT-RT impeller setup.

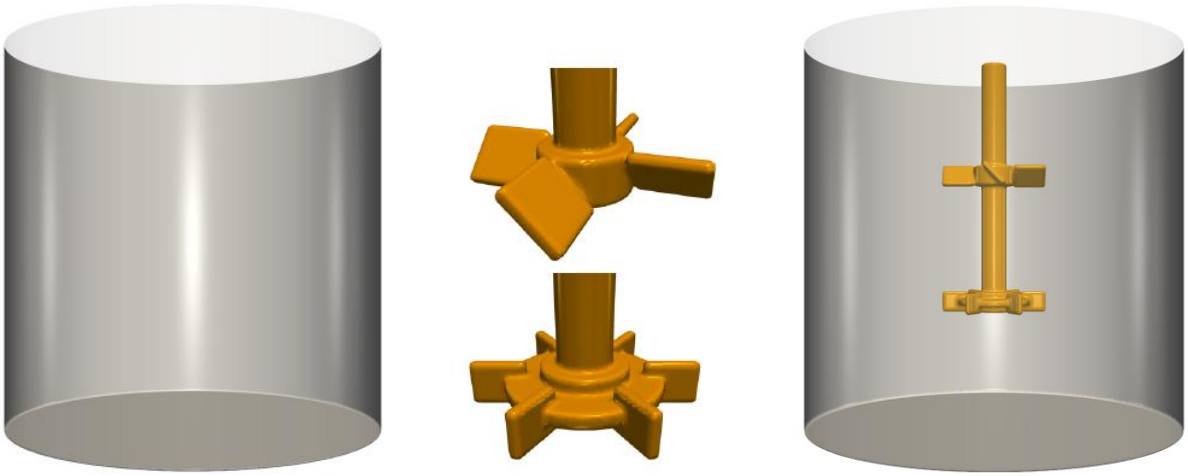

Figure 2. Numerical construction of all parts of the mixing system: (a) the cylindrical tank, (b) PBT and RT impellers (both D = 0.041 m), and (c) an example of a dual-impeller mixing system, containing both a PBT (upper) and an RT (lower) impeller.

3.2 Governing equations and numerical methods

This section concerns the numerical methods used in this study, which has been adapted from Russell *et al.* (2019). The mathematical model consists of solving the Navier-Stokes equations for the incompressible viscous fluids in a three-dimensional domain using Cartesian coordinates $\mathbf{x} = (x, y, z)$:

$$\nabla \cdot \mathbf{u} = 0 \tag{5}$$

$$\rho\left(\frac{\partial \mathbf{u}}{\partial t} + \mathbf{u} \cdot \nabla \mathbf{u}\right) = -\nabla p + \nabla \cdot \mu(\nabla \mathbf{u} + \nabla \mathbf{u}^T) + \rho \mathbf{g} + \mathbf{F_{fsi}} \tag{6}$$

where ρ is the density, t is the time, $\mathbf{u}$ is the velocity, p is the pressure, $\mathbf{g}$ is the gravitational acceleration and $\mathbf{F_{fsi}}$ is the solid-body force described by Fadlun *et al.* (2000), that has the advantage of keeping the accuracy and efficiency of the solution procedure. This force is defined numerically using the last step of the temporal integration of Eq. 6:

$$\rho \frac{\mathbf{u}^{n+1} - \mathbf{u}^n}{\Delta t} = \text{local} + \mathbf{F_{fsi}} \tag{7}$$

where "local" stands for the right hand side terms of Eq. 6, that contains the convective, pressure gradient, viscous, and gravitational force terms, and the superscripts denote the timestep. In the solid part of the domain (the impeller), $\mathbf{F_{fsi}}$ enforces the forced rotational motion $\mathbf{V^{n+1}}$:

$$\mathbf{u}^{n+1} = \mathbf{V}^{n+1} = 2\pi N\big((y - y_0) - (x - x_0)\big) \tag{8}$$

where (x_0, y_0) is the impeller central axis, N refers to rotational frequency and hence $\mathbf{F_{fsi}}$ is:

$$\mathbf{F_{fsi}} = \rho \frac{\mathbf{V}^{n+1} - \mathbf{u}^n}{\Delta t} - \text{local} \tag{9}$$

In summary, the impeller is considered as a fictive part in the Navier-Stokes solution (Eq. 6) when a force is applied. From Eq. 6, $\mu(\mathbf{x}, t)$ refers to the instantaneous local dynamic viscosity implemented explicitly and satisfies the Herschel-Bulkley model (Eq. 10 and Eq. 11).

$$\text{if } \dot{\gamma} > \dot{\gamma}_c \;\rightarrow\; \mu = \frac{\tau_y}{\dot{\gamma}} + K\left(\frac{\dot{\gamma}}{\dot{\gamma}_c}\right)^{n-1} \tag{10}$$

$$\text{if } \dot{\gamma} < \dot{\gamma}_c \;\rightarrow\; \mu = \tau_y \frac{\left(2 - \frac{\dot{\gamma}}{\dot{\gamma}_c}\right)}{\dot{\gamma}_c} + K\left((2-n) + (n+1)\frac{\dot{\gamma}}{\dot{\gamma}_c}\right) \tag{11}$$

where $\dot{\gamma}_c = 10^{-3}$ s^{-1} is the critical shear rate, or the value of the shear rate that corresponds to the fluid yield stress, and the other variables are as defined earlier. Inclusion of the $\dot{\gamma}_c$ term in Eq. 10 and 11 helps to avoid numerical instabilities caused by viscosity values approaching infinity at very low shear rate values when the material displays solid-like behaviour, by acting as a boundary between the solid behaviour and flowing regime. Due to the application of the piecewise equation, a reasonably accurate estimate of the critical shear rate is required for the fluid.

In addition to Eqs. 5-11, the boundary conditions applied to our system are as follows: non-slip on all solid objects (rotating impeller and fixed cylindrical tank) and stress-free on the top boundary ($w = 0$ and $du/dz = dv/dz = 0$). The code is fully parallelised and can run on various platforms from laptops to supercomputers. The parallelisation of the code is based on an algebraic domain decomposition technique (subdomains). The code is written in the computing language Fortran 2008 and the communication between processors is managed by data exchange across adjacent subdomains via the Messaging Passing Interface (MPI) protocol. The computational domain is cubic and discretized by a uniform fixed three-dimensional mesh using a finite-difference method. The calculation domain is divided into $3 \times 3 \times 3 = 27$ subdomains, where each subdomain holds a regular grid mesh of $64 \times 64 \times 64$ cells. The global resolution in the entire domain is then $192 \times 192 \times 192$. The mesh has a standard staggered MAC cell arrangement (Harlow and Welch (1965)), where the *u*, *v* and *w* velocity nodes are located on the corresponding cell faces and scalar variables are located at the cell centres. The Navier-Stokes equations are solved by a projection method (Chorin (1968); Temam (1968)) with incremental pressure correction (Goda (1979)) applied to a finite-difference scheme which has first- and second-order accuracy in time and space, respectively. In addition, a semi-implicit scheme is chosen for the velocities to relax the stability restriction on the time-step due to viscous diffusion. All spatial derivative operators are evaluated using standard centred-differences, except in the nonlinear term where we use a second-order Essentially-Non-Oscillatory (ENO) scheme (Shu and Osher (1989); Sussman *et al.* (1998)). See Russell *et al.* (2019) for details relating to a mesh dependency test carried out using an RT impeller.

Throughout this work, a cavern boundary definition of 0.01 m s^{-1} was selected. Other velocity magnitude values were tested, however it was confirmed via independent numerical trials that the definition of 0.01 m s^{-1} gave the best agreement with the experimental data. As a result, in all numerical velocity contour plots from this work, only velocity magnitude values ≥ 0.01 m s^{-1} are shown.

3.3 Numerical validation

In this work, CFD simulations were validated against the experimental study of Hirata *et al.* (1994), who investigated the mixing of a XG fluid with a 6-bladed RT impeller in a cylindrical tank fitted with four vertical baffles. Hirata *et al.* (1994) used LDA measurements to measure the azimuthal velocity profiles in the tank at a height, $z^* = 0.2$, where $z^* = -0.25$ referred to the bottom of the tank and $z^* = 0$ refers to the centre of the impeller, at four different *N* values ($N = 4$ s^{-1}, 5 s^{-1}, 7 s^{-1} and 11 s^{-1}). The numerical simulations were performed using the same setup as Hirata *et al.* (1994), at $N = 4$ s^{-1} and $N = 7$ s^{-1}, and azimuthal velocity profiles were obtained at $z^* \sim 0.15$-0.2 using post-processing software, Paraview. Good agreement between the experimental and numerical velocity profiles was obtained, with average absolute deviations per datum

(AAD) of 8.9% (R^2 = 0.952) and 13.1% (R^2 = 0.924), for the N = 4 s^{-1} and N = 7 s^{-1} runs, respectively. For further discussion relating to this validation process, the reader is directed to Russell *et al.* (2019).

4. Results and discussion

4.1 *Mixing Study A*: Rushton turbine-Rushton turbine (dual-RT)

In this section, we assess the mixing of a viscoplastic fluid with dual-RT system at different impeller separations, G. As stated in Table 2, G = 0.05 m (G/D = 1.22, *Mixing Study A(1)*) and G = 0.03 m (G/D = 0.73, *Mixing Study A(2)*), at a fixed lower impeller clearance, $C_2 = 1.10D$, were investigated. For the experimental studies, N was set to a low speed (N = 4.2 s^{-1}, Re_m = 2.7, Re_y = 1.0) and food dye was injected at the impeller tips. N was incrementally increased and the resulting caverns and flows were monitored. The experimental and numerical flows at five selected N values: N = 11.7 s^{-1} (Re_m = 13.0, Re_y = 8.1), N = 14.9 s^{-1} (Re_m = 18.9, Re_y = 13.3), N = 18.2 s^{-1} (Re_m = 25.6, Re_y = 19.7), N = 20.3 s^{-1} (Re_m = 30.5, Re_y = 24.7) and N = 33.3 s^{-1} (Re_m = 65.4, Re_y = 66.5) for each the impeller system can be visualised in Figure 3, with Rows (a) and (b) associated with *Mixing Study A(1)* and Rows (c) and (d) related to *Mixing Study A(2)*. When viscoplastic fluids are agitated with RT impellers, caverns with 'horn' torus morphology are formed. This morphology stems from the strongly radial nature of the RT impeller, with the impeller blades inducing centrifugal forces that push the material towards the tank wall. As the material reaches the cavern wall, conservation of mass results in the fluid recirculating back towards the centre of the vessel, producing vortices above and below the impeller blades.

In *Mixing Study A(1)*, there was strong compartmentalisation between the two caverns and flows over the range of N investigated. At lower N values, the stresses being applied to the fluid were not large enough to induce interaction between the two caverns (see Figure 3(a)(i)), resulting in the formation of two independent caverns. Interestingly, the upper one of the two caverns had a greater cavern aspect ratio than the lower one, with experimental cavern height-to-cavern diameter ratios, H_c/D_c = 0.53 and 0.44, respectively at N = 11.7 s^{-1} (Re_m = 13.0, Re_y = 8.1). The increased H_c in the upper cavern resulted in a decreased D_c, with respect to lower cavern, with an experimental dimensionless cavern diameter, D_c/D = 1.44 and 1.49 for the upper and lower caverns, respectively. It is hypothesised that this variation is caused by fluid agitation induced by the shaft both above and below the upper impeller, compared to shaft agitation solely above the lower impeller. As a result, the vortices above and below the upper impeller, and above the lower impeller were stretched in the z-direction, but the vortex below the lower impeller remained more compressed, as highlighted by the streamlines in the numerical result (Figure 3(b)(i)), leading to a slightly increased H_c/D_c and reduced D_c/D in the upper cavern. By further inspection of the numerical result at N = 11.7 s^{-1} (Re_m = 13.0, Re_y = 8.1), cavern interaction was observed. However, when the velocity was resolved into its component parts, focusing on the axial and azimuthal velocity profiles in the region between the impellers (Figure 4), cavern-cavern interaction, and associated fluid flow across impellers was seen to be unlikely. Figure 4(a) is the velocity field distribution within the vessel at N = 11.7 s^{-1} (Re_m = 13.0, Re_y = 8.1), with only flow at a velocity magnitude $\geq$ 0.01 m s^{-1} highlighted. The velocity profiles for the axial (u_z) and azimuthal (u_θ) components were taken along a vertical line (black line in Figure 4(a)), which extends from the top to the bottom of the vessel and passes the tips of both impellers, as seen in Figure 4(b) and (c). In the region between the impellers ($z \approx$ 0.066-0.082 m), which remains uncoloured in the experimental results, $u_\theta > 0.01$ m s^{-1}, whereas u_z, the component responsible for cavern-cavern interaction and cross-impeller fluid flow, is negligible by comparison, hence u_θ dominates the flow in this region, accounting for the observed discrepancy between the experimental and numerical results at N = 11.7 s^{-1} (Re_m = 13.0, Re_y = 8.1).

As N was increased in *Mixing Study A(1)*, the two caverns grew in size, interacting with one another to produce distinct compartmentalisation between the two flows and pronounced cavern-cavern segregation. When N reached 33.3 s^{-1} (Re_m = 65.4, Re_y = 66.5), the entire vessel contents was in motion, though clear segregation between the flows still existed despite the prominent deflection of the interface (Figure 3(a)(v)). The numerical results (Figure 3(b)(ii-v)) show that the vortices produced by both impellers are very similar in shape and size, leading to high levels of symmetry in the radial direction about the centre point between impellers. This symmetry results in the vortical behaviour below the upper RT blades

counteracting the vortices above the lower RT blades leading to the observed flow segregation. The formation of distinct cavern-cavern segregation in viscoplastic fluids agitated with sets of RT impellers is in agreement with the observed results of Arratia *et al.* (2006), who examined the agitation of Carbopol fluids with a 3-RT configuration (all D = 0.075 m and G = 0.09 m).

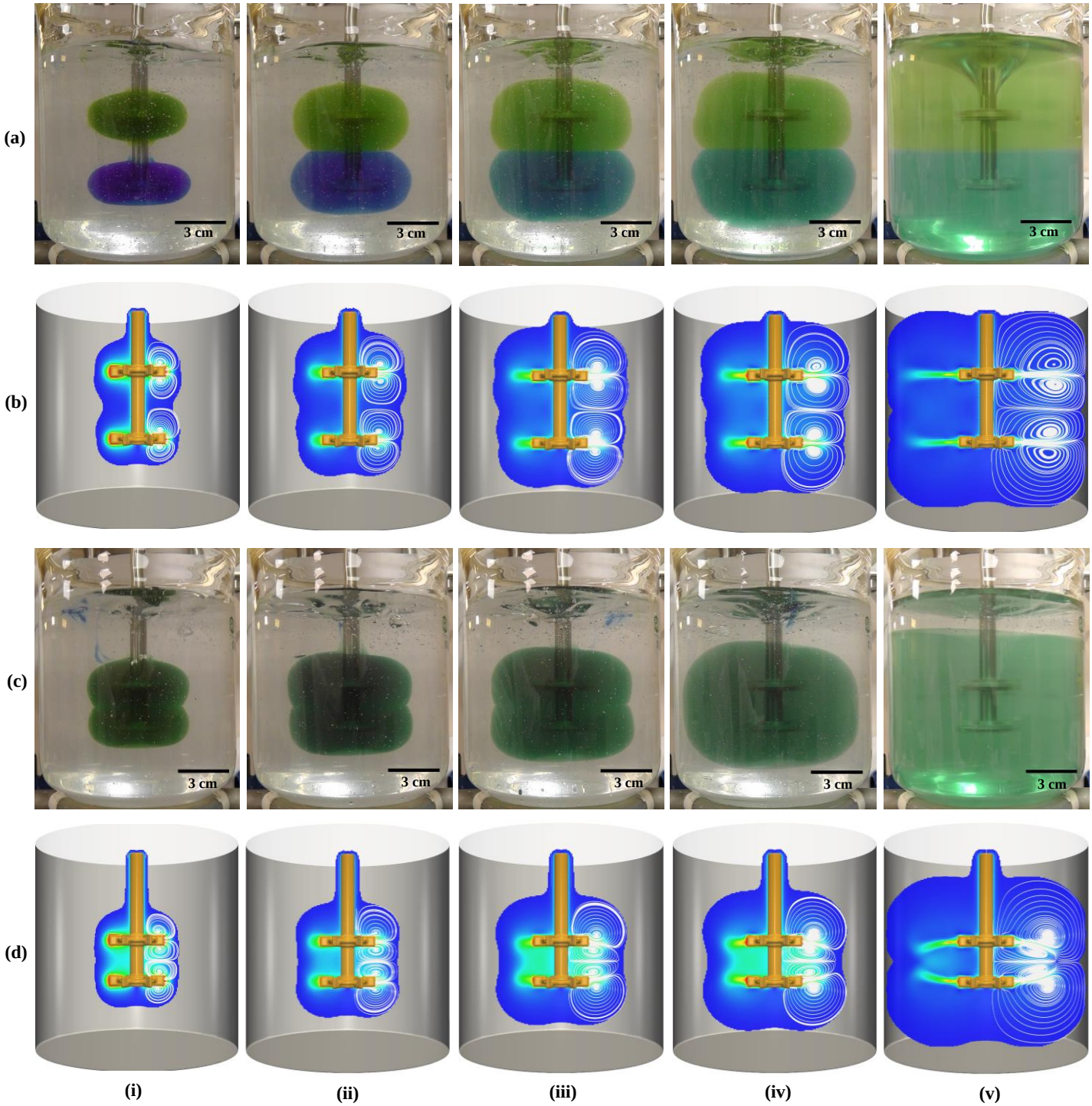

Figure 3. Experimental images and CFD snapshots for *Mixing Study A(1)* (Rows (a) and (b)) and *Mixing Study A(2)* (Rows (c) and (d), respectively). For both *Mixing Study A(1)* and *A(2)*, the following impeller rotational speeds, N were used in the images and snapshots: (i) 11.7 s^{-1} (Re_m = 13.0, Re_y = 8.1), (ii) 14.9 s^{-1} (Re_m = 18.9, Re_y = 13.3), (iii) 18.2 s^{-1} (Re_m = 25.6, Re_y = 19.7), (iv) 20.3 s^{-1} (Re_m = 30.5, Re_y = 24.7), and (v) 33.3 s^{-1} (Re_m = 65.4, Re_y = 66.5).

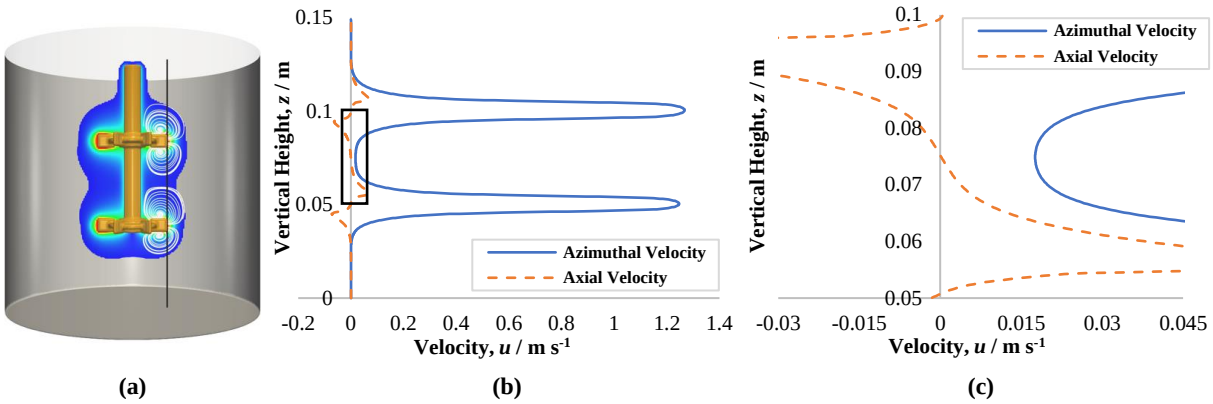

Figure 4. (a) Velocity field distribution within the vessel at N = 11.7 s^{-1} (Re_m = 13.0, Re_y = 8.1) in *Mixing Study A(1)*, with only flow at a velocity magnitude ≥ 0.01 m s^{-1} highlighted. The vertical black line at the impeller tips, which extends from the top to the bottom of the vessel, denotes where the in the vessel the azimuthal, u_θ and axial, u_z velocity profiles in (b) were taken from. (c) Close-up plot of the u_θ and u_z profiles for the region in the vessel between the centre of the two impellers (non-coloured in the experimental results), shown by the black box in (b).

The *Mixing Study A(1)* setup (G = 0.05 m, G/D = 1.22) was then utilised to investigate the effect of time on flow compartmentalisation, at N = 33.3 s^{-1} (Re_m = 61.5, Re_y = 70.7). The test C980 fluid had the rheological properties: τ_y = 26.4 Pa, K = 6.2 Pa s^n and n = 0.45 ($\dot{\gamma}$ range = 0.00059-963 s^{-1}, AAD = 1.97%, R^2 = 0.998), and green and blue food dye was injected into the top and bottom halves of the vessel contents, respectively at N = 3.33 s^{-1} (Re_m = 1.7, Re_y = 0.7). N was ramped up to 33.3 s^{-1} (Re_m = 61.5, Re_y = 70.7) to spread the dyes throughout the vessel. The motor was switched off, then back on, with images (Figure 5) taken at: (a) t = 0 s (immediately after the motor was switched on), (b) t = 148 s, (c) t = 267 s and (d) t = 368 s. At t = 0 s, there was limited transfer of material between the impellers, resulting in distinct compartmentalisation. Mixing between compartments increased with time until a homogenous state was reached at t = 368 s. It is hypothesised that this slow mass transfer resulted from the diffusion of dyed material from one compartment to the other, being swept into the flow patterns of the neighbouring compartment. This diffusion process was relatively slow compared to the rate of recirculation caused by agitation within each compartment, explaining why initially flow compartmentalisation was observed, before a state homogeneity was eventually achieved. Due to this time dependence, mixing with a dual-RT system would not be the recommended method for efficiently achieving homogeneity during the agitation of viscoplastic fluids.

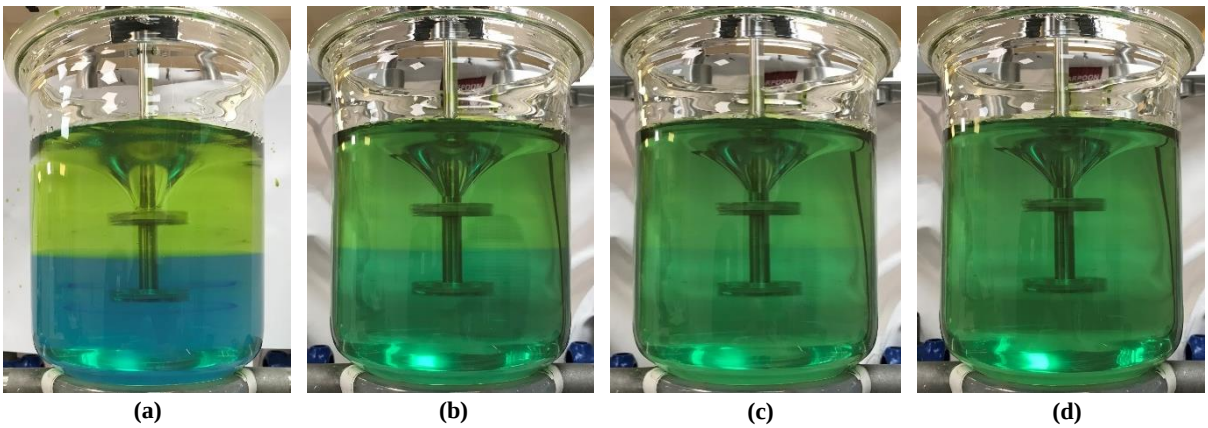

Figure 5. Mixing with the dual-RT system (G = 0.05 m, G/D = 1.22) at constant N = 33.3 s^{-1} (Re_m = 61.5, Re_y = 70.7). Going from (a) to (d) time, t is increasing: (a) t = 0 s, (b) t = 148 s, (c) t = 267 s, and (d) t = 368 s. t = 0 s indicates when N first reached 33.3 s^{-1}.

In *Mixing Study A(2)*, G was reduced to 0.03 m (G/D = 0.73) and over the entire range of N investigated, mixing between the two caverns was observed. In the experimental study, this was highlighted by the

homogeneous green/blue colour that formed in the regions of flow. In Figure 3(c)(i-iii), despite the homogeneous colour, distinctions between the two caverns were observed at the edges of the flows. It was hypothesised that this is likely to be caused by the u_z values being large enough to induce cross-impeller flow in the central part of the caverns; at the peripheries, u_θ greatly dominates over u_z and hence recirculation of material within the separate caverns is favoured over vertical mixing. The numerical results for the first three selected N values (Figure 3(d)(i-iii)) show that the velocity magnitudes are greater at the impeller region and between the impellers, than at the cavern periphery, aiding the observed mixing between impellers but flow compartmentalisation at the cavern edges from experiment. At N = 18.2 s^{-1} (Re_m = 25.6, Re_y = 19.7) in Figure 3(d)(iii), the lower vortex of the upper RT and the upper vortex of the lower RT are distinctly more compacted compared to the upper and lower vortices of the upper and lower RTs, respectively. This compaction becomes more pronounced with increasing N, until at N = 33.3 s^{-1} (Re_m = 65.4, Re_y = 66.5) in Figure 3(d)(v), where the upper and lower vortices of the upper and lower RT, respectively, encroach on the two central vortices and interact with one another. At N = 20.3 s^{-1} (Re_m = 30.5, Re_y = 24.7) in the experimental study (Figure 3(c)(iv)), it was hypothesised that the forces being applied to the material were large enough to induce sufficient cross-impeller flow for one continuous cavern to form and for the impellers to function as a single entity effectively. The result was the formation of a single cavern with approximately spherical morphology. This, however, was not predicted by the CFD model, where a cavern was produced (Figure 3(d)(iv)) that still had some segregation characteristics at the periphery. At N = 33.3 s^{-1} (Re_m = 65.4, Re_y = 66.5), the flowing material reached the tank wall (Figure 3(d and c)(v)), but the segregation characteristics still partially remained in the numerical results. Nevertheless, the observed stagnant zone near the top of the vessel was well predicted by the CFD model. It was surmised that the upper RT was too far from the interface to cause perturbation, resulting in a stagnant layer of material forming. Despite a substantial fraction of the material being well-mixed, complete homogeneity was not achieved throughout the vessel in *Mixing Study A(2)*.

4.2 *Mixing Study B*: Pitched-blade turbine-Pitched-blade turbine (dual-PBT)

Here, the mixing of a C980 fluid with a dual-PBT system (both D = 0.041 m) was evaluated at G = 0.05 m (G/D = 1.22, *Mixing Study B(1)*) and G = 0.03 m (G/D = 0.73, Mixing *Study B(2)*). Unlike the exclusively radial nature of RT impellers, PBT impellers produce flows with some axial character. Due to the rotational direction, the PBT impellers in this study are downward pumping, and there is a maxima in velocity magnitude (and hence force being exerted on the material) at a 45° angle to the radial direction at the blade tips. As a result, when a viscoplastic fluid is agitated by a PBT, the resulting cavern adopts an 'apple-shaped' torus, in contrast to the axisymmetic 'horn' torus shape produced by RT agitation (Xiao *et al.* (2014); Russell *et al.* (2019)). This is particularly evident at larger N values, when D_c is comparable to the tank diameter, T.

For both experimental studies in *Mixing Study B*, the impeller was set to N = 4.2 s^{-1} (Re_m = 2.5, Re_y = 1.1) and dye was injected at the tip of both impellers. N was then incrementally increased, with images capturing the flow at each N value. The experimental and numerical results at five selected speeds of N = 11.7 s^{-1} (Re_m = 12.2, Re_y = 8.3), 16.0 s^{-1} (Re_m = 19.8, Re_y = 15.5), 18.2 s^{-1} (Re_m = 24.1, Re_y = 20.0), 20.3 s^{-1} (Re_m = 28.7, Re_y = 25.1) and 33.3 s^{-1} (Re_m = 61.6, Re_y = 67.4) for both studies are presented in Figure 6, where Rows (a) and (b) relate to *Mixing Study B(1)*, and Rows (c) and (d) relate to *Mixing Study B(2)*.

In *Mixing Study B(1)*, two distinct caverns form at N = 11.7 s^{-1} (Re_m = 12.2, Re_y = 8.3), because the force being imparted on the material by the impellers was not great enough to induce cavern-cavern interaction (Figure 6(a)(i)). As before, the upper of the two caverns had a larger H_c/D_c and a smaller D_c due to the effects of shaft agitation. More specifically, H_c/D_c = 0.52 and 0.41, and D_c/D = 1.34 and 1.52, for the upper and lower cavern, respectively. The analogous numerical result (Figure 6(b)(i)) suggested cavern-cavern interaction occurred, however, as with *Mixing Study A(1)*, the u_θ component dominated flow in the region between the impellers which remained uncoloured via experiment, with u_z, the velocity component responsible for vertical mixing and cavern-cavern interaction, being negligible by comparison.

In Figure 6(a), as N increased from (ii) 16.0 s^{-1} (Re_m = 19.8, Re_y = 15.5) to (iv) 20.3 s^{-1} (Re_m = 28.7, Re_y = 25.1), there was interaction between the two caverns and noticeable cavern-cavern segregation. Both PBTs are downward-pumping, resulting in a lack of symmetry of the flows about the *x-y* plane at the

centre point between the impellers (if *z* is the vertical direction). This is in contrast to the dual-RT impeller system of *Mixing Study A(1)*, where the flows are axisymmetric about this central plane. As a result, the nature of flow compartmentalisation between the two studies was different. With increasing *N* from (ii) to (iv) in Figure 6(a), the rate of cavern growth of the lower cavern is faster than the upper cavern, with the upper cavern becoming increasingly faint in colour, whilst the lower cavern became progressively more green-blue in colour. It is hypothesised that despite the cavern-cavern segregation, small amounts of vertical mixing from upper to the lower cavern is occurring, due to the downward-pumping nature of the PBT. This material is then recirculated around the lower cavern but is unable to transfer back to the upper cavern. Conservation of mass results in the new material from just outside the upper cavern being drawn into its flow patterns, compensating for the material 'lost' from the upper to the lower cavern. Both the one-way vertical mixing and the new material being drawn in elucidate the aforementioned colour changes associated with both caverns. The observed cavern-cavern segregation is due to recirculation rates in the upper cavern being vastly superior to the vertical mixing rates from the upper to lower cavern, combined with the lower cavern being unable to transfer material back to the upper cavern. If the agitation system was symmetric about the aforementioned central *x-y* plane, the observed compartmentalisation would be stronger, with comparable cavern growth rates, similar to *Mixing Study A(1)*. For this to occur for a dual-PBT system, the pumping direction for the two PBT would have to be opposing, i.e. upward-downward or downward-upward for the upper and lower PBTs, respectively.

The analogous numerical results in Figure 6(b)(ii-iv) show that the observed experimental vertical mixing was not predicted by CFD, with stringent cavern-cavern segregation highlighted by the compartmentalisation of the sets of streamlines within the caverns. The result is a disparity between the predicted and observed cavern sizes and morphologies, with the predicted segregation resulting in the caverns growing at similar rates, with the lower cavern maintaining its 'apple' torus shape, which was not seen in the experimental study. However, the CFD model accurately predicted the upper cavern morphology over these *N* values. In *Mixing Study B(1)*, a phenomenon known as 'Newton's bucket' was observed, seen by the deflection of the material-air interface in Figure 6(a)(iii-v) and Figure 7. This was caused by a combination of the upper PBT being situated close to the interface and the downward-pumping nature of the PBT. However, the simulations were run for a single-phase system, and hence the stress-free assumption imposed on the upper boundary (as discussed in Section 3.2), applied to the corresponding simulations was no longer valid, leading to the observed deflection not being accounted for and likely owing to the discrepancies between the observed and predicted cavern morphologies and sizes.

From the experimental study, when $N = 33.3\ s^{-1}$ ($Re_m = 61.6$, $Re_y = 67.4$), the entirety of the vessel contents was in motion and well-mixed, owing to the observed homogeneous green-blue colour (Figure 6(a)(v)). As *N* increased from (iv) $N = 20.3\ s^{-1}$ ($Re_m = 28.7$, $Re_y = 25.1$) to (v) $N = 33.3\ s^{-1}$ ($Re_m = 61.6$, $Re_y = 67.4$), the lower cavern reached the tank wall, encroached upon and then engulfed the upper cavern to form one continuous, well-mixed cavern. This can be seen in Figure 7, which are two experimental images from *Mixing Study B(1)*, taken at $N = 25.0\ s^{-1}$ ($Re_m = 39.5$, $Re_y = 37.9$), with a ~5 s delay between (a) and (b). With increasing *N*, the volume of well-mixed fluid increased, until the full tank was in motion at (v) $N = 33.3\ s^{-1}$ ($Re_m = 61.6$, $Re_y = 67.4$). This engulfment process was well predicted by the CFD model, as seen by the streamlines connecting the lower and upper PBT in Figure 6(b)(v).

In *Mixing Study B(2)*, with $G = 0.03$ m ($G/D = 0.73$), the upper PBT was positioned further away from the fluid-air interface compared to *Mixing Study B(1)*. With this, over the investigated range of *N*, the force being exerted on the material by the upper PBT was not great enough to induce interface deflection, resulting in the stress-free assumption applied to the simulations being valid. However, there was still an inconsistency in cavern morphologies between the experimental (Figure 6(c)) and numerical (Figure 6(d)) results. In the experimental section, there was marked mixing between the two flows over the range of *N* investigated. From the initial dye injections, there were cavern-cavern interactions and dyed material flowed between the two impellers to form a continuous green-blue cavern. However, when *N* increased to (ii) $16.0\ s^{-1}$ ($Re_m = 19.8$, $Re_y = 15.5$), similar behaviour to *Mixing Study B(1)* was displayed. The downward-pumping characteristics of the upper PBT resulted in material flowing from the upper to the lower cavern, resulting in faster growth of the lower cavern, and faded coloration of the upper cavern. As *N* further increased to (iv) $N = 20.3\ s^{-1}$ ($Re_m = 28.7$, $Re_y = 25.1$), vertical mixing was able to occur in both directions, to form one continuous cavern of homogeneous green-blue colour.

When (v) $N = 33.3\ s^{-1}$ ($Re_m = 61.6$, $Re_y = 67.4$), the singular cavern reached the tank wall. However, due to the distance of the upper PBT from the interface, a stagnant zone of material was observed near the interface, so although the fluid was well-mixed within the cavern, only 80-90% of the vessel contents was in motion. When comparing to the respective numerical results (Figure 6(d)), there were noticeable differences in the cavern morphologies. At (i) $N = 11.7\ s^{-1}$ ($Re_m = 12.2$, $Re_y = 8.3$), the resulting flow was well predicted by the CFD model, with the streamlines showing vertical mixing from upper to the lower PBT, and recirculation back from the lower to the upper PBT. At (ii) $N = 16.0\ s^{-1}$ ($Re_m = 19.8$, $Re_y = 15.5$), experiment showed that the rate of material transfer from the upper to the lower PBT outweighed the recirculation back to the upper PBT from the lower. However, the numerical result suggests this rate of material transfer and the rate of recirculation are comparable and therefore the increased growth of the lower cavern, along with the loss of 'apple' torus character were not predicted by CFD. As a result, at (iii) $N = 18.2\ s^{-1}$ ($Re_m = 24.1$, $Re_y = 20.0$) and (iv) $N = 20.3\ s^{-1}$ ($Re_m = 28.7$, $Re_y = 25.1$), despite both experiment and CFD suggesting vertical mixing in both directions between the impellers and the formation of a singular, continuous cavern, the morphology of lower PBT flow remained toroidal due to the previous overestimation of the material recirculation from the lower to the upper PBT. By (v) $N = 33.3\ s^{-1}$ ($Re_m = 61.6$, $Re_y = 67.4$), the degree of both vertical mixing and recirculation is large enough for only two sets of streamlines to be generated. The model accurately predicted the fact that the cavern reached the tank wall and the development of a stagnant region at top of the vessel.

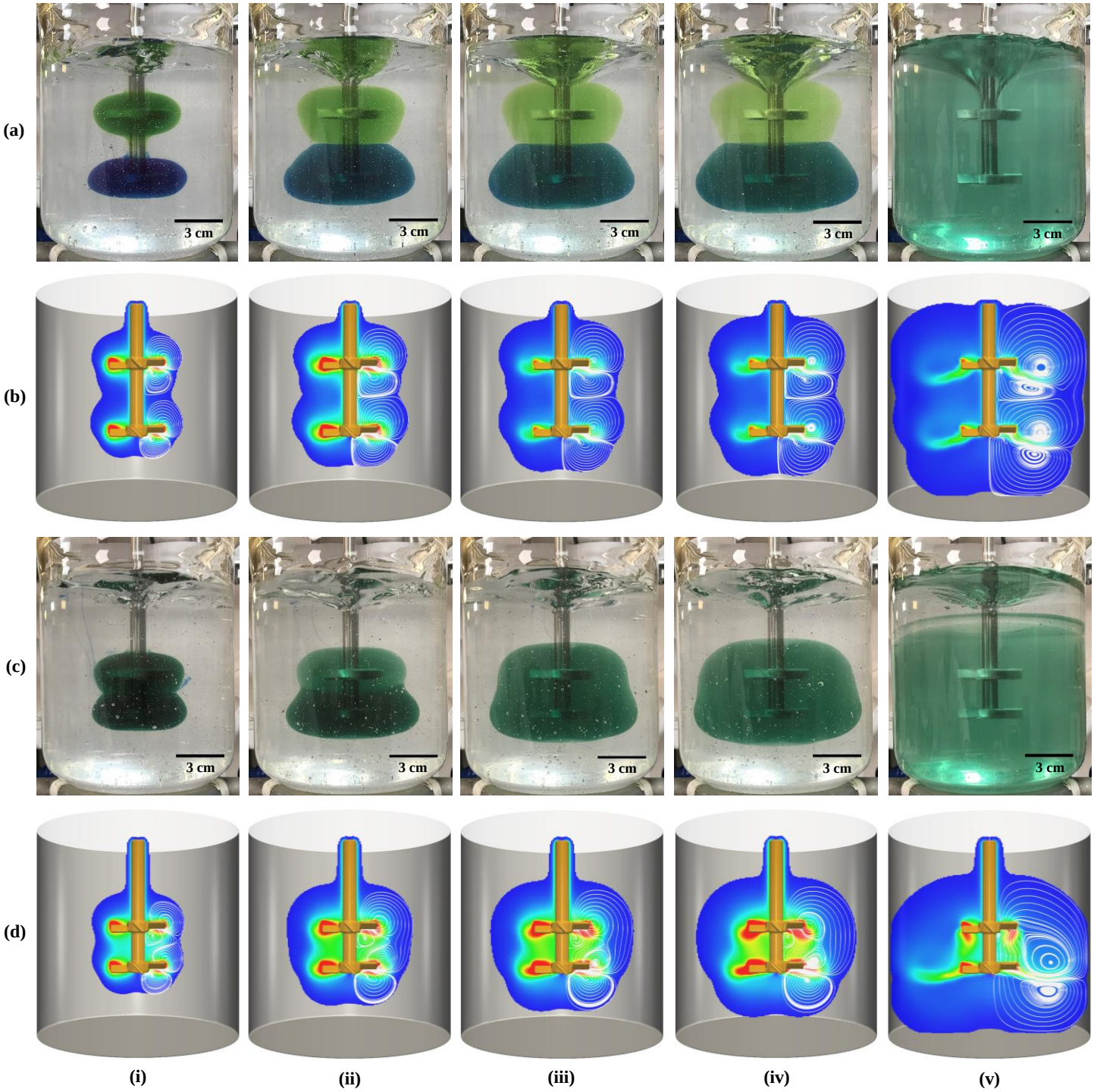

Figure 6. Experimental images and CFD snapshots for *Mixing Study B(1)* ((a) and (b), respectively) and *Mixing Study B(2)* ((c) and (d), respectively). For both *Mixing Study B(1)* and *B(2)*, the following impeller rotational speeds, *N* were used in the images and snapshots: (i) 11.7 s^{-1} (Re_m = 12.2, Re_y = 8.3), (ii) 16.0 s^{-1} (Re_m = 19.8, Re_y = 15.5), (iii) 18.2 s^{-1} (Re_m = 24.1, Re_y = 20.0), (iv) 20.3 s^{-1} (Re_m = 28.7, Re_y = 25.1), and (v) 33.3 s^{-1} (Re_m = 61.6, Re_y = 67.4).

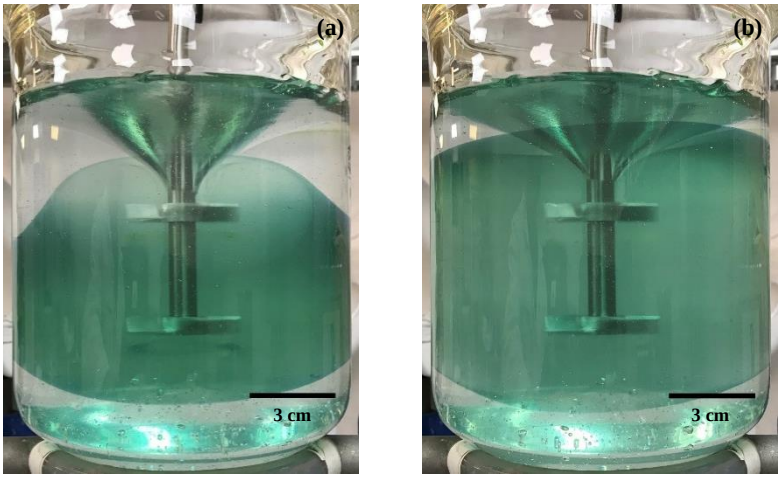

Figure 7. Experimental images from *Mixing Study B(1)*, taken at an impeller speed of N = 25.0 s^{-1} (Re_m = 39.5, Re_y = 37.9), with (a) taken approximately 5 s before (b). (a) Dynamic engulfment of the upper cavern by the lower cavern, and (b) the resulting single, homogeneous flow.

When a pair of vortices are rotated in the same direction, but lack axisymmetric characteristics, they will merge to form a single vortex (Tóth and Házi (2010)). However, if they rotate in the opposing direction, or in an axisymmetric fashion (as was the case in *Mixing Study A*), they will remain as a vortex dipole (Delbende and Rossi (2009)). In the case of *Mixing Study B(2)*, due to the downward pumping nature of the PBT impellers, the vortices above both impellers were rotating with the same characteristics, in an anti-clockwise direction. The impellers were close enough to result in the merging of these two vortices, to produce a single, large vortex. Consequently, the vortex below the upper impeller, which was rotating in a clockwise direction, was confined to the region near the rotating shaft, and resembled the vortex breakdown generated by rotating discs (Daube (1991); Spohn *et al.* (1993, 1998); Lopez *et al.* (1995, 2004); Piva and Meiburg (2005); Kahouadji and Martin Witkowski (2014)). As N increases, the size of this clockwise-rotating vortex decreases.

Comparing the results from both studies in *Mixing Study B*, there was better mixing between the two flows over a wider range of N in *Mixing Study B(2)*, though full-tank homogeneity was not achieved in this system. At sufficiently high N values in *Mixing Study B(1)*, cavern-cavern segregation was eliminated, resulting in the entire vessel contents being well-mixed. By comparison of the results from *Mixing Study A(1)* and *Mixing Study B(1)*, full-tank homogeneity was achievable using the dual-RT system if an appropriate amount of time was given for the diffusion process to occur. However, at comparable N, Re_m and Re_y values, this homogeneous state was achieved almost instantaneously with the dual-PBT setup. Therefore, to achieve full tank homogeneity in viscoplastic mixing processes using the lowest possible N, Re_m, Re_y and mixing times, agitation with the dual-PBT setup in *Mixing Study B(1)* appeared to be the superior method when comparing to the analogous dual-RT system of *Mixing Study A(1)*.

4.3 *Mixing Study C*: Combination of Rushton turbine and pitched-blade turbine (RT-PBT)

Finally, the mixing of a C980 fluid with an impeller system comprising of one RT and one PBT was evaluated. In *Mixing Study C(1)*, the upper impeller was a RT and the lower impeller was a PBT, with G = 0.05 m (G/D = 1.22). In *Mixing Study C(2)*, the setup was reversed, whilst G = 0.05 m (G/D = 1.22) was retained. The fluid agitated in both systems had the Herschel-Bulkley parameters: τ_y = 32.6 Pa, K = 8.6 Pa s^n and n = 0.43 (see Table 1, Section 2.1 for further details). For both experimental studies, dye injection occurred at N = 4.2 s^{-1} (Re_m = 1.8, Re_y = 0.9). The experimental and numerical flows at five selected N values: N = 11.7 s^{-1} (Re_m = 9.3, Re_y = 7.0), 16.0 s^{-1} (Re_m = 15.2, Re_y = 13.2), 18.2 s^{-1} (Re_m = 18.6, Re_y = 17.0), 20.3 s^{-1} (Re_m = 22.2, Re_y = 19.1) and 33.3 s^{-1} (Re_m = 48.2, Re_y = 57.3), for *Mixing Study C(1)* and *Mixing Study C(2)*, can be seen in Figure 8(a) and (b), and Figure 8(c) and (d), respectively.

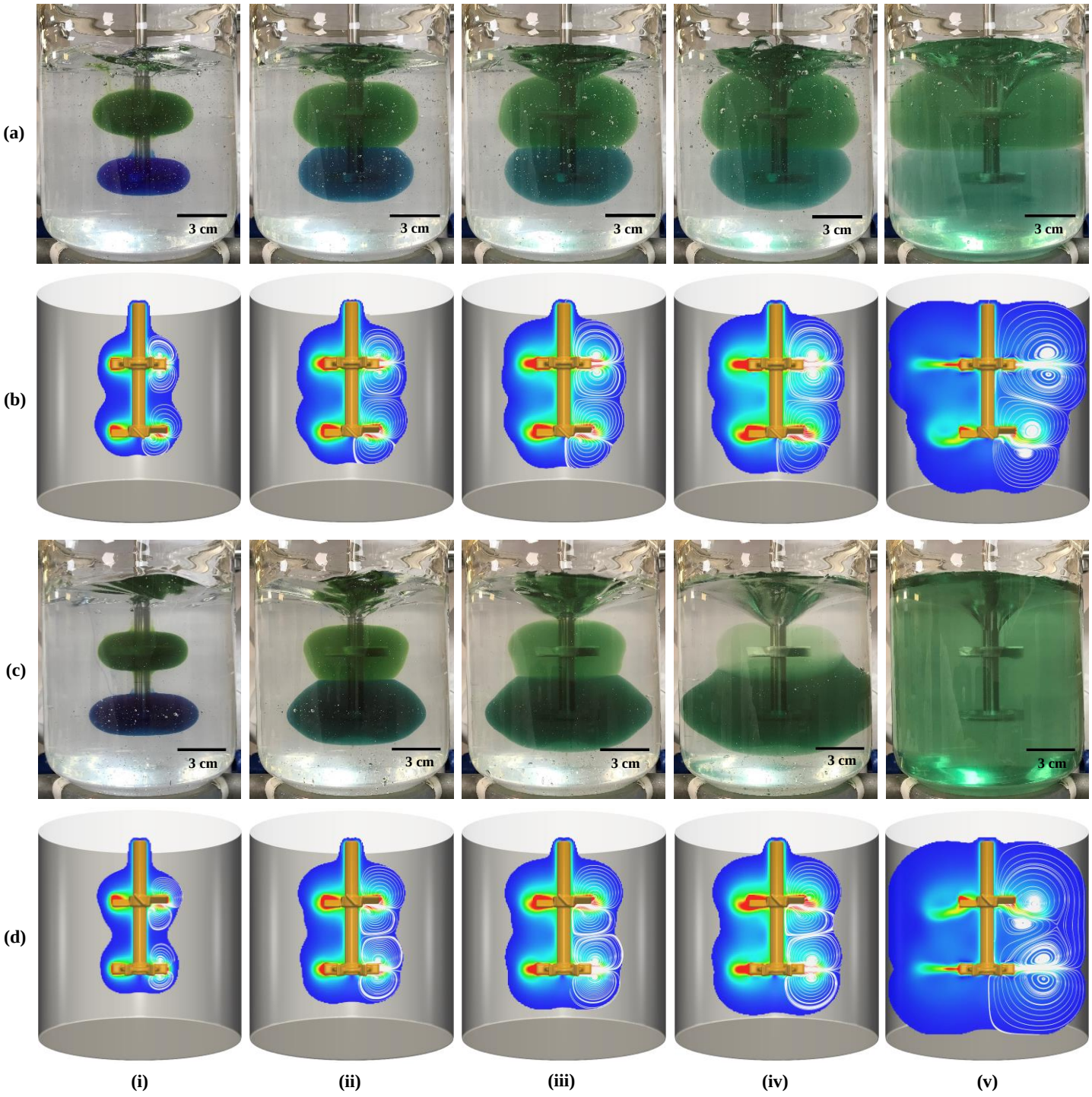

Figure 8. Experimental images and CFD snapshots for *Mixing Study C(1)* ((a) and (b), respectively) and *Mixing Study C(2)* ((c) and (d), respectively). For both *Mixing Study C(1)* and *C(2)*, the following N values were used in the images and snapshots: (i) 11.7 s^{-1} (Re_m = 9.3, Re_y = 7.0), (ii) 16.0 s^{-1} (Re_m = 15.2, Re_y = 13.2), (iii) 18.2 s^{-1} (Re_m = 18.6, Re_y = 17.0), (iv) 20.3 s^{-1} (Re_m = 22.2, Re_y = 19.1), and (v) 33.3 s^{-1} (Re_m = 48.2, Re_y = 57.3).

From the experimental results of *Mixing Study C(1)* (Figure 8(a)), distinct cavern-cavern segregation was observed over the range of investigated N. As with all G = 0.05 m (G/D = 1.22) mixing studies in this work, at (i) N = 11.7 s^{-1} (Re_m = 9.3, Re_y = 7.0), cavern-cavern interaction was unable to occur, resulting in two independent caverns forming. The upper RT produced a larger cavern than the lower PBT, with

a D_c/D = 1.51 and an H_c/D_c = 0.48 for the RT-agitated cavern, compared to a cavern of D_c/D = 1.39 and H_c/D_c = 0.41 produced by the PBT. Russell *et al.* (2019) previously showed that for a given fluid agitated at a specific N, the RT produced a cavern with greater D_c than the PBT. It was hypothesised earlier in this work, that due to the effects of shaft rotation, the upper cavern often has a larger H_c/D_c but smaller D_c than the lower cavern. However, in this case, the fact that the RT is able to create larger caverns at a given N than the PBT outweighs the effects of shaft rotation, resulting in the upper cavern having both a greater H_c/D_c and D_c than the lower cavern at N = 11.7 s^{-1} (Re_m = 9.3, Re_y = 7.0). In Figure 8(b)(i), cavern-cavern interaction was predicted numerically for the aforementioned reasons.

As previously discussed, RT impellers have solely radial character, with a maximum in velocity magnitude at the tip of the impeller blades. In contrast, the PBT has axial character, with a maximum in velocity magnitude at the impeller tips in a 45° downward direction. Therefore, through PBT agitation, similar vortices are produced to those seen through RT agitation, however now at this 45° angle. For both the RT and PBT, due to the shear-thinning nature of the material, the fluid recirculating around the edges of the caverns will have relatively low, but comparable velocity values. As a result, when these flows meet at the cavern-cavern boundary in the *Mixing Study C(1)* setup, there is not enough force exerted by either impeller to induce significant transfer of material from one cavern to the other, leading to flow compartmentalisation and cavern-cavern segregation. When N was increased to (v) 33.3 s^{-1} (Re_m = 48.2, Re_y = 57.3), both caverns reached the tank wall and the majority of the vessel is in motion, but the flow compartmentalisation remained. These findings were relatively well predicted by the CFD simulations, as seen by the distinction between the sets of streamlines in Figure 8(b), over all N investigated. The simulations also correctly predicted that as N increased, the cavern produced by RT agitation grew slightly faster than the PBT cavern and that at (v) N = 33.3 s^{-1} (Re_m = 48.2, Re_y = 57.3), there were some stagnant zones near the tank wall, in particular at the bottom of the tank. As seen previously, interface deflection (Newton's bucket) was observed in Figure 8(a)(iii-v). This behaviour was not accommodated for numerically and could account for any potential discrepancies in cavern morphology and size when comparing the experimental and numerical results. In a similar manner to *Mixing Study A(1)*, if the flow was agitated at N = 33.3 s^{-1} (Re_m = 48.2, Re_y = 57.3) for a sufficient time, mixing between the caverns through diffusion would occur. However, as was the case in *Mixing Study A(1)*, if the aim of the viscoplastic mixing process is to produce homogeneity throughout the vessel at reduced mixing times, then the dual-RT(upper)-PBT(lower) system presented here would not be the recommended setup.

From the experimental findings in *Mixing Study C(2)* (Figure 8(c)), at (i) N = 11.7 s^{-1} (Re_m = 9.3, Re_y = 7.0), the expected lack of interaction between the two caverns was observed. The lower cavern, agitated with the RT, had a D_c/D = 1.66 and an H_c/D_c = 0.39, whilst the PBT-induced upper cavern had a D_c/D = 1.37 and an H_c/D_c = 0.45. These results agreed with the aforementioned findings that the RT produces larger D_c values at a given N and fluid rheology than the PBT (dominant effect), in conjunction with the lower cavern often having a greater D_c, but a smaller H_c/D_c, due to shaft agitation effects. The numerical result in Figure 8(d)(i) suggested cavern-cavern interaction for the same reasons as previously discussed. As N increased to (v) N = 33.3 s^{-1} (Re_m = 48.2, Re_y = 57.3) in the experimental study, similar behaviour was observed to that seen in the dual-PBT system from *Mixing Study B(1)*. At (ii) N = 16.0 s^{-1} (Re_m = 15.2, Re_y = 13.2) and (iii) N = 18.2 s^{-1} (Re_m = 18.6, Re_y = 17.0), vertical mixing of material from the downward-pumping axial flow of the PBT to the lower cavern occurred, with the RT unable to transfer material back to upper cavern. The result was faster growth rates of the lower cavern than the upper cavern, the increased green-blue colour of the lower cavern and the green colour of the upper cavern becoming increasingly faint as new, uncoloured material was drawn into the flow patterns of the upper cavern. Cavern-cavern segregation was seen due to recirculation rates in the upper cavern dominating over the rate of material transfer to the lower cavern, in conjunction with the inability of the RT to transfer material back to the upper cavern. As N increased, the dynamic engulfment process of the upper cavern by the lower cavern was again observed, until full-tank homogeneity occurred at (v) N = 33.3 s^{-1} (Re_m = 48.2, Re_y = 57.3). Comparing the numerical and experimental results in *Mixing Study C(2)*, vertical mixing from the upper cavern to the lower cavern was not predicted via CFD, and therefore faster growth rates of lower cavern in experiment were not accounted for in the simulations, leading to the similar growth rates of both caverns. However, at (v) N = 33.3 s^{-1} (Re_m = 48.2, Re_y = 57.3), the vertical mixing in the upward and downward directions was correctly predicted by CFD, leading to the near-full tank homogeneity being seen in both the numerical and experimental results.

As before, interface deflection (Newton's bucket) was not accounted for in the CFD model, which could be an explanation for the discrepancies between the experimental and numerical results.

Comparison of the results of *Mixing Study C(2)* and *Mixing Study B(1)*, shows that similar flow behaviour was exhibited in these mixing cases. The fluid used in *Mixing Study C(2)* had a larger τ_y and K, and had a slightly more shear-thinning nature than the fluid used in *Mixing Study B(1)*. Due of this, it was expected that the encroachment and engulfment process would start (i.e. when the lower cavern has $D_c \approx T$) at a lower N and therefore a lower Re_m and Re_y in *Mixing Study B(1)*, than in *Mixing Study C(2)*. However the reverse is true, with $N \approx 19.0$ s^{-1} ($Re_m \approx 19.9$, $Re_y \approx 18.6$) for *Mixing Study C(2)*, compared to $N \approx 22.0$ s^{-1} ($Re_m \approx 32.4$, $Re_y \approx 29.4$) for *Mixing Study B(1)*. This may be because the RT produces larger caverns than the PBT, for a given N and fluid rheology. As a result, at a fixed G and fluid rheology, lower N, Re_m and Re_y values are required to achieve full-tank homogeneity in the PBT(upper)-RT(lower) system of *Mixing Study C(2)*, compared to the dual-PBT system of *Mixing Study B(1)*. Therefore, and comparing to the results from all mixing studies in this work, the PBT(upper)-RT(lower), $G = 0.05$ m ($G/D = 1.22$) system of *Mixing Study C(2)* seemed to produce the best mixing in terms of achieving full vessel homogeneity at the lowest N, Re_m, Re_y and mixing times.

4.4 Quantitative comparisons

In this section, quantitative comparisons are made between the cavern dimensions that result from agitation by the various impeller configurations in *Mixing Studies A-C*. Depending on the impeller configuration in question, the D_c/D values that resulted for upper and lower caverns varied. As previously discussed, in *Mixing Studies A(1), B(1), C(1)* and *C(2)*, $G = 0.05$ m ($G/D = 1.22$), compared to $G = 0.03$ m ($G/D = 0.73$) in *Mixing Studies A(2)* and *B(2)*. For the $G = 0.03$ m ($G/D = 0.73$) systems, mixing between the upper and lower flows occurred over the entire range of investigated N, however for the $G = 0.05$ m ($G/D = 1.22$) systems, at lower N values the stresses being exerted on the material by the impellers were not great enough to induce interactions between the two flows, resulting in the formation of two independent caverns. For *Mixing Studies A(1)* and *C(1)*, where the upper impeller was the RT, cavern-cavern interaction was first seen at $N = 13.8$ s^{-1} ($Re_m = 16.8$, $Re_y = 11.4$), compared to $N = 14.9$ s^{-1} ($Re_m = 18.9$, $Re_y = 13.3$) for *Mixing Studies B(1)* and *C(2)* where the upper impeller was the PBT.

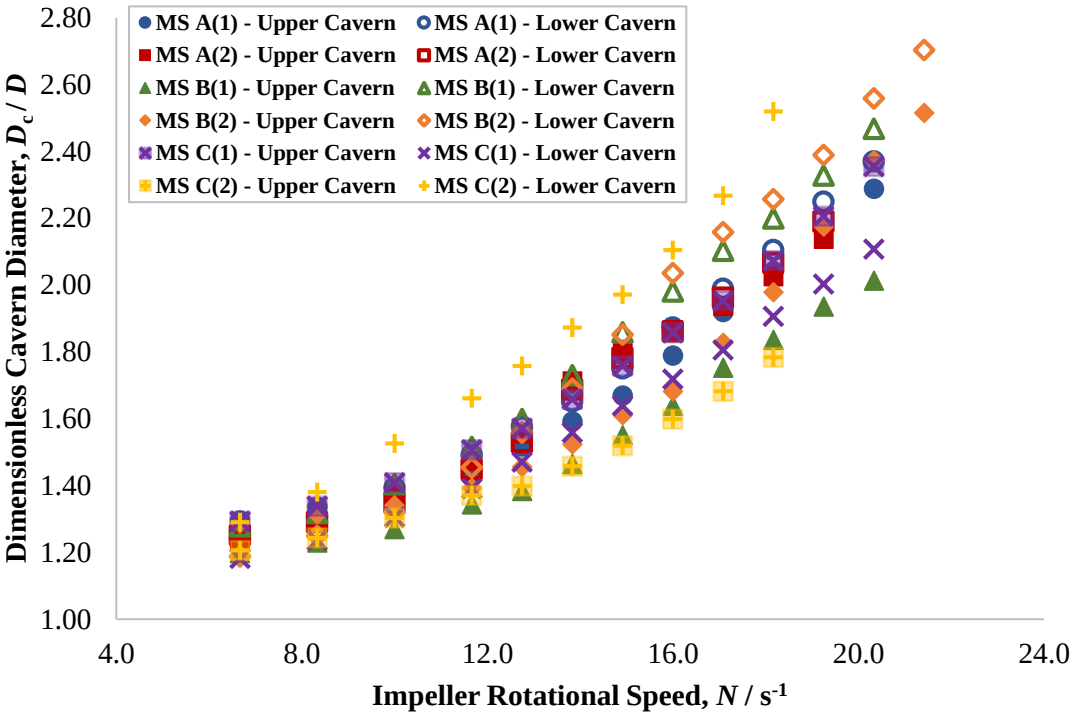

Figure 9. Experimentally-derived dimensionless cavern diameters, D_c/D plotted against impeller rotational speed, N for the upper and lower caverns that resulted from agitation by the various impeller configurations from all mixing studies in this work.

Figure 9 is a plot of D_c/D values over the ranges of investigated N for each of the mixing studies in this work. D_c/D values were measured for all caverns until $D_c = T$, or until the previously mentioned cavern engulfment process occurred. For the G = 0.05 m (G/D = 1.22) mixing studies, even when cavern-cavern interactions occurred, distinct individual cavern characteristics remained at the peripheries of both caverns, allowing D_c/D values for the upper and lower flows to be measured throughout this regime. Individual cavern characteristics were also seen in the G = 0.03 m (G/D = 0.73) systems, despite the mixing of flows over all N values. As seen in Figure 9, for all systems, as N increased, the D_c/D values of the upper and lower caverns increased. Due to shaft agitation effects, the lower cavern generally had a larger D_c than the upper cavern, and there was no discontinuous jump in D_c/D when cavern-cavern interaction occurred in the G = 0.05 m (G/D = 1.22) systems. However, for *Mixing Study C(1)*, where the upper and lower impellers were the RT and PBT impellers, respectively, the upper cavern had larger D_c values than the lower cavern over the range of investigated N. As discussed in previous sections and in Russell *et al.* (2019), when mixing a given fluid at a specific scale and N value, a cavern resulting from RT agitation will have a larger D_c than a cavern produced by agitation with a PBT impeller of similar dimensions. In the case of *Mixing Study C(1)*, this effect outweighed the effects of the shaft agitation (as discussed in Section 4.1). In the dual-RT, G = 0.03 m (G/D = 0.73) system of *Mixing Study A(2)*, both the upper and lower flows grew in size at comparable rates due to the highly symmetrical nature of the flows (Figure 3), however in the dual-PBT, G = 0.03 m (G/D = 0.73) system of *Mixing Study B(2)*, the lower flow grew at a faster rate than the upper flow at low N values, due to the downward pumping nature of the PBT allowing for unidirectional transfer of material from the upper to the lower flow, with limited recirculation being observed back to the upper flow (Figure 6). Hence, the lower flow had larger D_c/D values than the upper flow over the entire range of N.

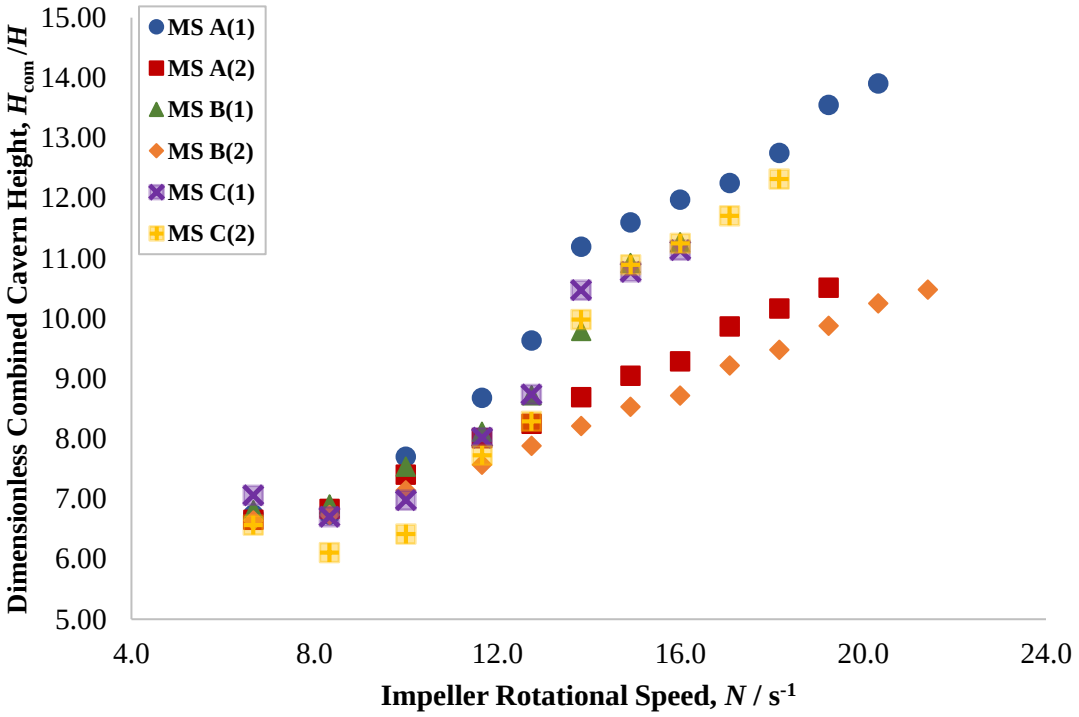

Figure 10. Experimentally-derived dimensionless combined cavern heights, H_{com}/H plotted against impeller rotational speed, N for the caverns that resulted from agitation by the various impeller configurations from all mixing studies in this work.

Figure 10 is a plot of the combined cavern heights of the upper and lower caverns produced in each of the mixing studies, H_{com}, non-dimensionalised by the impeller height, H, against the individual ranges of N. For the G = 0.03 m (G/D = 0.73) systems, there was an almost linear relationship between H_{com}/H and N, caused by the mixing of the upper and lower flows over the entire range of investigated N in both systems. However, for the G = 0.05 m (G/D = 1.22) systems, there was a discontinuous increase in H_{com}/H when the two distinct caverns went from a state of being independent to a state of cavern-cavern interaction at N = 13.8 s^{-1} (Re_m = 16.8, Re_y = 11.4) for *Mixing Studies A(1)* and *C(1)*, and N = 14.9 s^{-1} (Re_m = 18.9, Re_y = 13.3) for *Mixing Studies B(1)* and *C(2)*. Data were analysed until the upper cavern reached the interface, or until either cavern reached the tank wall. As would be expected, due to the greater impeller separations, at larger N values, the H_{com}/H values in the G = 0.05 m (G/D = 1.22) systems were significantly larger than in the G = 0.03 m (G/D = 0.73) systems.

5. Conclusions

In this study, dye visualisation techniques in conjunction with a validated CFD model were used to characterise the flow of Carbopol 980 (C980) fluids in a 2 L vessel equipped with various dual-impeller systems. The C980 solutions exhibited viscoplastic rheological properties, and were agitated with different combinations of 6-bladed Rushton turbine (RT) impellers and 4-bladed 45° pitched-blade turbine (PBT) impellers (impeller diameter, D = 0.041 m), with the lower impeller positioned at an impeller clearance-to-impeller diameter ratio, C_1/D = 1.10, in all cases. Three mixing studies were performed. In *Mixing Study A*, a dual-RT impeller system was used, at impeller separations, G = 0.05 m (G/D = 1.22) and G = 0.03 m (G/D = 0.73), whilst *Mixing Study B* focused on dual-PBT impeller systems with the same G values. *Mixing Study C* looked at a combination of the RT and the PBT, with the RT as the upper impeller in *Mixing Study C(1)* and the PBT as the upper impeller in *Mixing Study C(2)*, with G = 0.05 m (G/D = 1.22) in both cases.

In *Mixing Study A*, mixing with the dual-RT, G = 0.05 m (G/D = 1.22) system led to distinct cavern-cavern segregation and flow compartmentalisation over the range of impeller speeds, N investigated,

which was well predicted by the CFD model. A similar C980 fluid was then agitated with the same impeller setup, at a constant N = 33.3 s^{-1} (Re_m = 61.5, Re_y = 70.7) and the cavern-cavern segregation was found to be a time dependent process, with a state of full-vessel homogeneity being achieved after ~6 min. In the dual-RT, G = 0.03 m (G/D = 0.73) system, mixing between the caverns occurred over the range of N investigated, with a stagnant layer forming near the interface at N = 33.3 s^{-1} (Re_m = 65.4, Re_y = 66.5), which was well predicted by CFD.

In *Mixing Study B*, due to the downward pumping nature of the PBT, although noticeable cavern-cavern segregation remained in the G = 0.05 m (G/D = 1.22) system, vertical mixing from the upper to the lower cavern occurred, resulting in faster cavern growth rates of the lower flow. At higher N values, the lower cavern encroached upon and engulfed the upper cavern, to form a continuous, homogeneous flow. The vertical mixing was not predicted by CFD, resulting in the increased rate of growth of the lower cavern not being projected. However, at higher N, mixing between the two caverns was forecasted by CFD. For the dual-PBT, G = 0.03 m (G/D = 0.73) system, at a relatively low N value, slight cavern-cavern segregation was witnessed, before a continuous, homogeneous flow was seen at higher N values. As with the dual-RT, G = 0.03 m (G/D = 0.73), a stagnant zone of material formed at the top of the vessel, due to the distance of the upper PBT from the interface. The analogous numerical results over-predicted the degree of recirculation of material from the lower to the upper PBT at low N values, resulting in the faster growth of the lower cavern not being accounted for and hence there were differences in cavern morphology between the experimental and numerical results. The stagnant zone at the top of the vessel was well predicted.

In *Mixing Study C*, the RT(upper)-PBT(lower) system produced similar cavern-cavern segregation to *Mixing Study A(1)* dual-RT, G = 0.05 m (G/D = 1.22) system, over the range of investigated N, which was forecasted by the CFD model. The PBT(upper)-RT(lower) system displayed very similar behaviour to the dual-PBT, G = 0.05 m (G/D = 1.22) system, resulting in full-tank homogeneity at higher N values. The CFD did not predict the vertical mixing between caverns at lower N values, and hence the faster growth of the lower cavern compared to the upper cavern. However, full tank homogeneity at higher N values was projected well numerically. Throughout the study, the effects of interface deflection on cavern size and morphology were not accounted for by the CFD model, due to the stress-free condition imposed on the upper boundary. It was concluded that for dual-impeller, viscoplastic mixing, the PBT(upper)-RT(lower), G = 0.05 m (G/D = 1.22) setup from *Mixing Study C(2)* resulted in the best mixing, in terms of full-tank homogeneity being achieved with the lowest mixing times, N, Re_m and Re_y values.

Quantitative comparisons of the results from all mixing studies showed that the lower caverns had a larger dimensionless cavern diameter, D_c/D than the upper caverns at each given N value, except in *Mixing Studies A(2)* and *C(1)*. In *Mixing Study C(1)*, the shaft agitation effects were outweighed by the lack of downward pumping capability by the RT from the upper to the lower cavern and the fact that RT impellers produce larger caverns than comparable PBT impellers in a given mixing system setup. In *Mixing Study A(2)*, the caverns grew at comparable rates due to the symmetrical nature of the flow. The dimensionless combined cavern heights, H_{com}/H profiles of each system showed a discontinuous increase in H_{com}/H caused by cavern-cavern interaction in the G = 0.05 m (G/D = 1.22) systems, not seen in the G = 0.03 m (G/D = 0.73) systems.

Future work should consider the inclusion of a fluid-air interface into the CFD model, which would assist in capturing the interface deflection observed in the experiments and, therefore, minimise the discrepancies observed between the experimental and numerical results.

Acknowledgements

The authors would like to thank Syngenta Ltd for funding this work through a PhD CASE studentship. This work is also supported by the UK Engineering and Physical Sciences Research Council (EPSRC) [grant numbers EP/M507878/1, EP/K003976/1]. Special thanks to Patricia Carry for granting permission for use of the Anton Paar MCR 302, and Andrew Quarmby, Neil Gibson, Anita Rea and John Hone for their technical expertise and assistance throughout this work. We thank with gratitude Richard Craster for helpful numerical discussion. The numerical simulations were performed with code BLUE (Shin et al. (2017)) and run using the high-performance computing resources provided by the Research

Computing Service (RCS) of Imperial College London. Data supporting this publication can be obtained on request from cep-lab@imperial.ac.uk.

Nomenclature

A_b	Blade angle [°]
C	Impeller clearance [m]
C_1	Upper impeller clearance [m]
C_2	Lower impeller clearance
D	Impeller diameter [m]
D_c	Cavern diameter [m]
D_d	Disc diameter [m]
D_h	Hub diameter [m]
F_{fsi}	Solid-body force [N]
G	Impeller separation [m]
g	Gravitational acceleration [m s^{-2}]
H	Impeller height [m]
H_L	Liquid fill height [m]
H_b	Blade height [m]
H_c	Cavern height [m]
H_{com}	Combined cavern height [m]
H_h	Hub height [m]
K	Flow consistency index [Pa s^n]
k_s	Impeller geometry constant [-]
L_b	Blade length [m]
N	Impeller rotational speed [s^{-1}]
N_b	Blade number [-]
n	Flow behaviour index [-]
p	Pressure [Pa]
P	Power input [W]
R	Tank radius [m]
Re_m	Modified power-law Reynolds number [-]
Re_y	Yield stress Reynolds number [-]
S	Shaft diameter [m]
T	Tank Diameter [m]
T_b	Blade Thickness [m]
T_d	Disc Diameter [m]
t	Time [s]
u	Velocity [m s^{-1}]
u_z	Axial velocity component [m s^{-1}]
u_θ	Azimuthal velocity component [m s^{-1}]
V	Tank Volume [L]
W_b	Blade width [m]

Greek Letters

$\dot{\gamma}$	Shear rate [s^{-1}]
$\bar{\dot{\gamma}}$	Mean shear rate [s^{-1}]
$\dot{\gamma}_c$	Critical shear rate [s^{-1}]
μ	Fluid viscosity [Pa s]
ρ	Fluid density [kg m^{-3}]
τ	Shear stress [Pa]
τ_y	Fluid yield stress [Pa]
Ψ	Static distance function [-]

References

Adams, L.W., Barigou, M., 2007. CFD analysis of caverns and pseudo-caverns developed during mixing of non-Newtonian fluids. Chem. Eng. Res. Des. 85, 598-604

Alvarez, M.M., Zalc, J.M., Shinbrot, T., Arratia, P.E., Muzzio, F.J., 2002. Mechanisms of mixing and creation of structure in laminar stirred tanks. AIChE J. 48, 2135–2148.

Amanullah, A., Hjorth, S.A., Nienow, A.W., 1998a. A new mathematical model to predict cavern diameters in highly shear thinning, power-law liquids using axial-flow impellers. Chem. Eng. Sci. 53, 455–469.

Amanullah, A., Hjorth, S.A., Nienow, A.W., 1997. Cavern sizes generated in highly shear thinning viscous fluids by SCABA 3SHP1 impellers. Food Bioprod. Process. 75, 232–238.

Amanullah, A., Serrano-Carreon, L., Castro, B., Galindo, E., Nienow, A.W., 1998b. The influence of impeller type in pilot scale Xanthan fermentations. Biotechnol. Bioeng. 57, 95–108.

Ameur, H., Bouzit, M., Ghenaim, A., 2015. Numerical study of the performance of multistage Scaba 6SRGT impellers for the agitation of yield stress fluids in cylindrical tanks. J. Hydrodyn. 27, 436–442.

Arratia, P.E., Kukura, J., Lacombe, J., Muzzio, F.J., 2006. Mixing of shear-thinning fluids with yield stress in stirred tanks. AIChE J. 52, 2310–2322.

Aubin, J., Xuereb, C., 2006. Design of multiple impeller stirred tanks for the mixing of highly viscous fluids using CFD. Chem. Eng. Res. Des. 61, 2913–2920.

Balmforth, N.J., Frigaard, I.A., Ovarlez, G., 2014. Yielding to stress: Recent developments in viscoplastic fluid mechanics. Annu. Rev. Fluid Mech. 46, 121–146.

Barry, B.W., Meyer, M.C., 1979. The rheological properties of Carbopol gels I. Continuous shear and creep properties of Carbopol gels. Int. J. Pharm. 2, 1–25.

Baudou, C., Xuereb, C., Bertrand, J., 1997. 3-D Hydrodynamics generated in a stirred vessel by a multiple-propeller system. Can. J. Chem. Eng. 75, 653–663.

Bujalski, W., Jaworski, Z., Nienow, A.W., 2002. CFD Study of homogenisation with dual Rushton turbines - Comparison with experimental results Part II: The multiple reference frame. Chem. Eng. Res. Des. 80, 97–104.

Chorin, A.J., 1968. Numerical solution of the Navier-Stokes Equations. Math. Comput. 22, 745–762.

Cortada-Garcia, M., Weheliye, W.H., Dore, V., Mazzei, L., Angeli, P., 2018. Computational fluid dynamic studies of mixers for highly viscous shear thinning fluids and PIV validation. Chem. Eng. Sci. 179, 133–149.

Daube, O., 1991. Numerical simulation of axisymmetric vortex breakdown in a closed cylinder, in: Anderson, C.R., Greengard, C. (Eds.), Lectures in Applied Mathematics Vol. 28. American Chemical Society, pp. 131–152.

Delbende, I., Rossi, M., 2009. The dynamics of a viscous vortex dipole. Phys. Fluids 21, 073605-1–15.

Dinkgreve, M., Paredes, Denn, M.M., Bonn, D., 2016. On different ways of measuring “the” yield stress. J. Nonnewton. Fluid Mech. 238, 233–241.

Elson, T.P., 1988. Mixing of fluids possessing a yield stress, in: 6th European Conference on Mixing. Pavia, pp. 485–492.

Elson, T.P., Cheesman, D.J., Nienow, A.W., 1986. X-Ray Studies of Cavern Sizes and Mixing Performance with Fluids Possessing a Yield Stress. Chem. Eng. Sci. 41, 2555–2562.

Fadlun, E.A., Verzicco, R., Orlandi, P., Mohd-Yusof, J., 2000. Combined immersed-boundary finite-difference methods for three-dimensional complex flow simulations. J. Comput. Phys. 161, 35–60.

Galindo, E., Argüello, M.A., Velasco, D., Albiter, V., Martínez, A., 1996. A comparison of cavern development in mixing a yield stress fluid by Rushton and Intermig impellers. Chem. Eng. Technol. 19, 315–323.

Galindo, E., Nienow, A.W., 1993. Performance of the scaba 6SRGT agitator in mixing of simulated xanthan gum broths. Chem. Eng. Technol. 16, 102–108.

Galindo, E., Nienow, A.W., 1992. Mixing of highly viscous simulated Xanthan fermentation broths with the Lightnin A-315 Impeller. Biotechnol. Prog. 8, 233–239.

Goda, K., 1979. A Multistep Technique with implicit difference schemes for calculating two- or three-dimensional cavity flows. J. Comput. Phys. 30, 79–95.

Harlow, F.H., Welch, J.E., 1965. Numerical calculation of time-dependent viscous incompressible Flow of fluid with free surface. Phys. Fluids 8, 2182–2189.

Herschel, W.H., Bulkley, R., 1926. Konsistenzmessungen von gummi-benzollösungen. Colloid Polym. Sci. 39, 291–300.

Hirata, Y., Nienow, A.W., Moore, I.P.T., 1994. Estimation of cavern sizes in a shear-thinning plastic fluid agitated by a Rushton turbine based on LDA measurements. J. Chem. Eng. Japan 27, 235–237.

Hui, L.K., Bennington, C.P.J., Dumont, G.A., 2009. Cavern formation in pulp suspensions using side-entering axial-flow impellers. Chem. Eng. Sci. 64, 509–519.

Ihejirika, I., Ein-Mozaffari, F., 2007. Using CFD and ultrasonic velocimetry to study the mixing of pseudoplastic fluids with a helical ribbon impeller. Chem. Eng. Technol. 30, 606–614.

Jaworski, Z., Bujalski, W., Otomo, N., Fellow, A.W.N., 2000. CFD Study of homogenization with dual Rushton turbines - Comparison with experimental results Part I: Initial studies. Chem. Eng. Res. Des. 78, 327–333.

Jaworski, Z., Pacek, A.W., Nienow, A.W., 1994. On flow close to cavern boundaries in yield stress. Chem. Eng. Sci. 49, 3321-3324

Kahouadji, L., Martin Witkowski, L., 2014. Free surface due to a flow driven by a rotating disk inside a vertical cylindrical tank: Axisymmetric configuration. Phys. Fluids 26, 072105-1–17.

Kahouadji, L., Nowak, E., Kovalchuk, N., Chergui, J., Juric, D., Shin, S., Simmons, M.J.H., Craster, R. V, Matar, O.K., 2018. Simulation of immiscible liquid – liquid flows in complex microchannel geometries using a front ‐ tracking scheme. Microfluid. Nanofluidics 22, 1–12.

Kazemzadeh, A., Ein-Mozaffari, F., Lohi, A., Pakzad, L., 2017. Intensification of mixing of shear-thinning fluids possessing yield stress with the coaxial mixer composed of two different Central Impellers and an Anchor. Chem. Eng. Process. Process Intensif. 111, 101–114.

Kazemzadeh, A., Ein-Mozaffari, F., Lohi, A., Pakzad, L., 2016a. -Effect of the rheological properties on the mixing of Herschel-Bulkley fluids with coaxial mixers: Applications of tomography, CFD, and response surface methodology. Can. J. Chem. Eng. 94, 2394–2406.

Kazemzadeh, A., Ein-Mozaffari, F., Lohi, A., Pakzad, L., 2016b. A new perspective in the evaluation of the mixing of biopolymer solutions with different coaxial mixers comprising of two dispersing impellers and a wall scraping anchor. Chem. Eng. Res. Des. 114, 202–219.

Kelly, W.J., Humphrey, A.E., 1998. Computational fluid dynamics model for predicting flow of viscous fluids in a large fermentor with hydrofoil flow impellers and internal cooling coils. Biotechnol. Prog. 14, 248–258.

Letellier, B., Xuereb, C., Swaels, P., Hobbes, P., Bertrand, J., 2002. Scale-up in laminar and transient regimes of a multi-stage stirrer, a CFD approach. Chem. Eng. Sci. 57, 4617–4632.

Lopez, J.M., 1995. Unsteady swirling flow in an enclosed cylinder with reflectional symmetry. Phys.

Fluids 7, 2700–2714.

Lopez, J.M., Marques, F., Hirsa, A.H., Miraghaie, R., 2004. Symmetry breaking in free-surface cylinder flows. J. Fluid Mech. 502, 99–126.

Malkin, A., Kulichikhin, V., Ilyin, S., 2017. A modern look on yield stress fluids. Rheol. Acta 56, 177–188.

Metzner, A.B., Feehs, R.H., Ramos, H.L., Otto, R.E., Tuthill, J.D., 1961. Agitation of viscous Newtonian and non-Newtonian fluids. AIChE J. 7, 3–9.

Metzner, A.B., Otto, R.E., 1957. Agitation of non-Newtonian fluids. AIChE J. 3, 3–10.

Montante, G., Magelli, F., 2004. Liquid homogenization characteristics in vessels stirred with multiple Rushton turbines mounted at different spacings: CFD study and comparison with experimental data. Chem. Eng. Res. Des. 82, 1179–1187.

Oppong, F.K., Rubatat, L., Frisken, B.J., Bailey, A.E., De Bruyn, J.R., 2006. Microrheology and structure of a yield-stress polymer gel. Phys. Rev. E 73, 041405-1–9.

Pakzad, L., Ein-Mozaffari, F., Chan, P., 2008a. Using computational fluid dynamics modeling to study the mixing of pseudoplastic fluids with a Scaba 6SRGT impeller. Chem. Eng. Process. Process Intensif. 47, 2218–2227.

Pakzad, L., Ein-Mozaffari, F., Chan, P., 2008b. Measuring mixing time in the agitation of non-Newtonian fluids through electrical resistance tomography. Chem. Eng. Technol. 31, 1838–1845.

Pakzad, L., Ein-Mozaffari, F., Chan, P., 2008c. Using electrical resistance tomography and computational fluid dynamics modeling to study the formation of cavern in the mixing of pseudoplastic fluids possessing yield stress. Chem. Eng. Sci. 63, 2508–2522.

Pakzad, L., Ein-Mozaffari, F., Upreti, S.R., Lohi, A., 2013a. Agitation of Herschel–Bulkley fluids with the Scaba–anchor coaxial mixers. Chem. Eng. Res. Des. 91, 761–777.

Pakzad, L., Ein-Mozaffari, F., Upreti, S.R., Lohi, A., 2013b. Experimental and numerical studies on mixing of yield-pseudoplastic fluids with a coaxial mixer. Chem. Eng. Commun. 200, 1553–1577.

Pakzad, L., Ein-Mozaffari, F., Upreti, S.R., Lohi, A., 2013c. A novel and energy-efficient coaxial mixer for agitation of non-Newtonian fluids possessing yield stress. Chem. Eng. Sci. 101, 642–654.

Papanastasiou, T.C., 1987. Flows of materials with yield. J. Rheol. 31, 385–404.

Patel, D., Ein-Mozaffari, F., Mehrvar, M., 2012. Improving the dynamic performance of continuous-flow mixing of pseudoplastic fluids possessing yield stress using Maxblend impeller. Chem. Eng. Res. Des. 90, 514–523.

Piau, J.M., 2007. Carbopol gels: Elastoviscoplastic and slippery glasses made of individual swollen sponges. Meso- and macroscopic properties, constitutive equations and scaling laws. J. Nonnewton. Fluid Mech. 144, 1–29.

Piva, M., Meiburg, E., 2005. Steady axisymmetric flow in an open cylindrical container with a partially rotating bottom wall. Phys. Fluids 17, 063603-1–12.

Russell, A.W., Kahouadji, L., Mirpuri, K., Quarmby, A., Piccione, P.M., Matar, O.K., Luckham, P.F., Markides, C.N., 2019. Mixing viscoplastic fluids in stirred vessels over multiple scales: A combined experimental and CFD approach. Chem. Eng. Sci. 208, 115129:1–16.

Saeed, S., Ein-Mozaffari, F., 2008. Using dynamic tests to study the continuous mixing of xanthan gum solutions. J. Chem. Technol. Biotechnol. 83, 559–568.

Saeed, S., Ein-Mozaffari, F., Upreti, S.R., 2008. Using computational fluid dynamics to study the dynamic behavior of the continuous mixing of Herschel-Bulkley fluids. Ind. Eng. Chem. Res. 47, 7465–7475.

Saeed, S., Ein-Mozaffari, F., Upreti, S.R., 2007. Using computational fluid dynamics modeling and ultrasonic doppler velocimetry to study-pulp suspension mixing. Ind. Eng. Chem. Res. 46, 2172–2179.

Shin, S., Chergui, J. and Juric, D., 2017. A solver for massively parallel direct numerical simulation of three-dimensional multiphase flows. J. Mech. Sci. and Tech. 31 (4), 1739–1751.

Shu, C.-W., Osher, S., 1989. Efficient implementation of essentially non-oscillatory shock-capturing schemes, II. J. Comput. Phys. 83, 32–78.

Solomon, J., Elson, T.P., Nienow, A.W., Pace, G.W., 1981. Cavern sizes in agitated fluids with a yield

stress. Chem. Eng. Commun. 11, 143–164.

Sossa-Echeverria, J., Taghipour, F., 2015. Computational simulation of mixing flow of shear thinning non-newtonian fluids with various impellers in a stirred tank. Chem. Eng. Process. 93, 66–78.

Sossa-Echeverria, J., Taghipour, F., 2014. Effect of mixer geometry and operating conditions on flow mixing of shear thinning fluids with yield stress. AIChE J. 60, 1156–1167.

Spohn, A., Mory, M., Hopfinger, E.J., 1998. Experiments on vortex breakdown in a confined flow generated by a rotating disc. J. Fluid Mech. 370, 73–99.

Spohn, A., Mory, M., Hopfinger, E.J., 1993. Observations of vortex breakdown in an open cylindrical container with a rotating bottom. Exp. Fluids Exp. Methods their Appl. to Fluid Flow 14, 70–77.

Sussman, M., Fatemi, E., Smereka, P., Osher, S., 1998. An improved level set method for incompressible two-phase flow. Comput. Fluids 27, 663–680.

Temam, R., 1968. An approximation method for solving Navier-Stokes equations. B Soc Math Fr 96, 115.

Tóth, G., Házi, G., 2010. Merging of shielded Gaussian vortices and formation of a tripole at low Reynolds numbers. Phys. Fluids 22, 053101-1–7.

Vrabel, P., van der Lans, R.G.J.M., Luyben, K.C.A.M., Boon, L., Nienow, A.W., 2000. Mixing in large-scale vessels stirred with multiple radial or radial and axial up-pumping impellers: Modelling and measurements. Chem. Eng. Sci. 55, 5881–5896.

Wichterle, K., Wein, O., 1981. Threshold of mixing of non-Newtonian liquids. Int. Chem. Eng. 21, 116–120.

Xiao, Q., Yang, N., Zhu, J., Guo, L., 2014. Modeling of cavern formation in yield stress fluids in stirred tanks. AIChE J. 60, 3057–3070.